NORGES TEKNISK-NATURVITENSKAPELIGE
UNIVERSITET

Lecture Notes on the Numerical Solution of Stochastic Differential Equations

by
A. Naess

PREPRINT
STATISTICS NO. 11/2001
ISSN 0804-9173

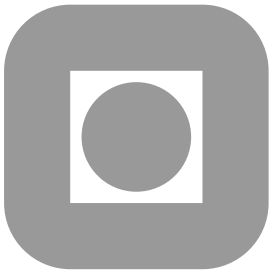

NORWEGIAN UNIVERSITY OF SCIENCE AND
TECHNOLOGY
TRONDHEIM, NORWAY

This report has URL
http://www.math.ntnu.no/preprint/statistics/2001/S11-2001.ps
Arvid Naess has homepage: http://www.math.ntnu.no/∼arvidn
E-mail: arvidn@math.ntnu.no
Address: Department of Mathematical Sciences, Norwegian University of Science and Technology, N-7491 Trondheim, Norway.

Postgraduate Course on Numerical Methods
for Stochastic Differential Equations
Lund University, 7 - 11 May 2001

—

Lecture Notes on the Numerical Solution of Stochastic Differential Equations by Path Integration Methods

A. Naess
Department of Mathematical Sciences
Norwegian University of Science and Technology
NO-7491 Trondheim, Norway
arvidn@math.ntnu.no

1 INTRODUCTION

In these lecture notes the focus will be on so-called path integration methods for calculating the probability law of the solution of stochastic differential equations (SDE). The goal then becomes that of calculating the joint probability density function (PDF) of the phase space Markov vector process that solves the nonlinear SDE. It is known that for a large class of SDEs, the joint PDF satisfies the so-called Fokker-Planck (FP) equation [1]. Over the years a considerable amount of effort has been directed toward establishing methods for solving this equation. In recent years the shift has clearly been toward numerical methods of solution. Based on past experience, it is clearly recognized that it is still a formidable challenge to solve the FP equation for higher dimensional problems. For such problems analytical solutions are known only for a restricted class of nonlinear stochastic systems [2, 3, 4].

The development of numerical solution procedures seems to have followed mainly three different lines of attack. Of these, the most generally applicable approaches seem to be based on finite element (FE) techniques, which provides weak solutions to the FP equation, see e.g. [5, 6, 7, 8], and the path integration (PI) method, cf. e.g. [9, 10, 11, 12, 13]. The use of Galerkin type methods for calculating weak solutions of Fokker-Planck equations by means of orthogonal expansions have also been pursued [14, 15, 16, 17, 18]. The basic limitation

of these numerical procedures are the dimension of the problems that can be solved. So far, only 4D problems have been partly solved. Still the accuracy of the obtained numerical solutions in the tail regions of the PDFs are somewhat uncertain.

Among the first systematic efforts to develop the PI method into a numerical tool are those of Wehner & Wolfer [19, 20, 21]. Naess & Johnsen [10, 11] showed that the PI method could be implemented in such a manner that extremely accurate results could be obtained for the tail behaviour of the joint PDF of the state space vector for both 2D and 3D cases. This makes the PI method of particular interest for the estimation of extreme responses of dynamical systems which can be modelled as nonlinear oscillators excited by forces, external or parametric, that can be approximated as white noise or filtered white noise processes.

The purpose of these lectures is to describe the basic principles underlying the path integration method and some recent developments concerning the numerical implementation of the PI method.

2 THE FROBENIUS-PERRON OPERATOR

Even the simplest, most inconspicuous transformation $S : X \to X$, where X denotes a specified state space (e.g. $X = [0, 1]$), may exhibit irregular (chaotic) behaviour resembling in many respects random behaviour. The logistics transformation $S : [0, 1] \to [0, 1]$ defined by $S(x) = 4x(1 - x)$ is one of the classical examples of such a transformation [22, 23]. Starting from an initial point x_0 say, the transformation will produce the trajectory $x_0, x_1 = S(x_0), x_2 = S(x_1), \ldots$.

A specific feature of the logistics transformation is the existence of a stationary density. This can be observed (and estimated) by running a Monte Carlo simulation in the following manner: The transformation S is used to propagate forward in time a large number of initial states, $x_0^{(i)}, i = 1, 2, \ldots, N$, which are distributed according to some initial density $f_0(x)$. After a sufficient number of iterations, n say, the density $f_n(x)$ of the n'th iterates $x_n^{(i)}, i = 1, \ldots, N$ approximates the stationary density which we denote by $f_*(x)$. An estimate of the stationary density based on $N = 5000$ is shown in Figure 1.

Another approach is to show that S gives rise to an operator P which maps the space of densities defined on X into itself (a more rigorous definition is given below). The action of P is to propagate the corresponding densities instead of individual points. That is, $P^n f_0 = f_n$. The operator P is called the Frobenius-Perron (FP) operator. Its defintion in a general setting is as follows [24].

Let $(X, \mathcal{F}, \mu)$ be a measure space, and let $L^1 = L^1(X, \mathcal{F}, \mu)$ denote the space of (complex) integrable functions [25]. $D = D(X, \mathcal{F}, \mu) = \{f \in L^1, f \geq$

$0, \|f\| = 1\}$ = the space of densities. Here $\|f\| = \int_X |f(x)|\mu(dx)$.

Let $S : X \to X$ be a measurable transformation, that is $S^{-1}(A) \in \mathcal{F}$ for all $A \in \mathcal{F}$. S is called nonsingular if $\mu(S^{-1}(A)) = 0$ for every $A \in \mathcal{F}$ such that $\mu(A) = 0$, that is, the transformation S does not collapse non-null sets into null sets.

Let $S : X \to X$ be a nonsingular transformation. The unique operator $P : L^1 \to L^1$ defined by the equation

$$\int_A Pf(x)\,\mu(dx) = \int_{S^{-1}(A)} f(x)\,\mu(dx) \quad \text{for every } A \in \mathcal{F}, \tag{1}$$

is called the Frobenius-Perron operator associated with S. It is easy to see that $P : D \to D$

In mathematical language, the existence of a stationary density can be rephrased into saying that the associated Frobenius-Perron operator P has a fixed point $f_*(x)$ ($f_* \in D \subset L^1$), i.e. $Pf_* = f_*$

In the context of the logistics transformation, the FP operator is defined by the equation

$$\int_\Delta Pf(x)\,dx = \int_{S^{-1}(\Delta)} f(x)\,dx \tag{2}$$

where Δ is a measurable subset of $X = [0, 1]$, which is equipped with Lebesgue measure.

It can be shown [24] that the FP operator associated with the logistics transformation can in fact be given explicitly as follows:

$$Pf(x) = \frac{1}{4\sqrt{1-x}}\{f(\,[1-\sqrt{1-x}\,]/2) + f(\,[1+\sqrt{1-x}\,]/2) \tag{3}$$

Ulam and von Neuman [26] succeeded in actually finding a closed form expression for the stationary density for the logistics transformation above by exploiting the FP operator. They proved the nontrivial result

$$f_*(x) = \frac{1}{\pi\sqrt{x(1-x)}} \tag{4}$$

which can be seen to agree closely with the empirical density plotted in Figure 2. In general, one cannot expect to be able to derive an explicit and closed-form expression for the stationary density.

Hence, in practice, there are two alternative approaches for estimating the stationary density. 1) By following the evolution in time of a large number of

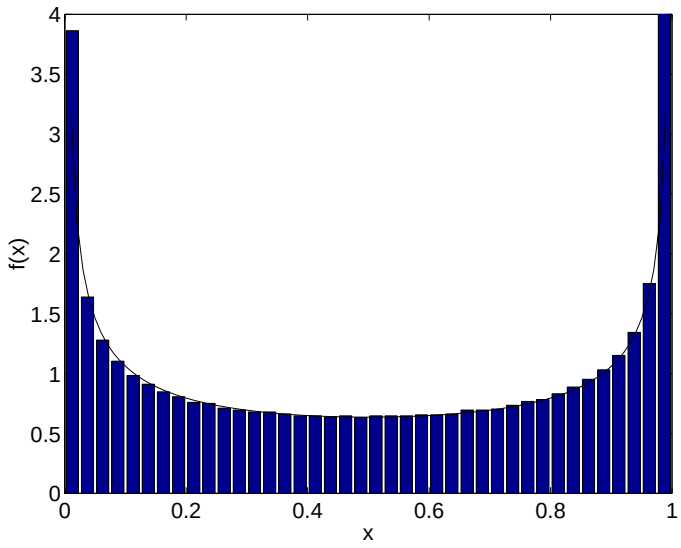

Figure 1: Empirical stationary density for the logistics transformation. The full drawn line is the theoretical stationary density given by equation (4).

initial states by iterating S. 2) Or, directly by following the evolution in time of an initial density by iterating the FP operator P.

It is realized that by changing the focus from the transformation S to the associated FP operator P, the perspective has been lifted from the details of individual trajectories to a study coined in a probabilistic language of the overall beaviour of the states. This is our first example of a PI method, which was developed here for a purely deterministic system with chaotic behaviour. It does, however, display the general character of the PI method also for stochastic systems. In order to extend the PI method to also encompass such systems, it is necessary to look at a more general class of operators than the FP operators.

3 MARKOV OPERATORS

The FP operator is a 'deterministic' operator. To be able to handle also stochastic dynamic problems, it is required to introduce more general operators than above, viz. the Markov operators [24].

Let $(X, \mathcal{F}, \mu)$ be a (sigma-finite) measure space. Any linear operator $P : L^1 \to L^1$ satisfying the following properties

(1) $Pf \geq 0$ for $f \geq 0$, $f \in L^1$

(2) $\|Pf\| = \|f\|$ for $f \geq 0$, $f \in L^1$

is called a Markov operator. Hence, any linear operator $P : L^1 \to L^1$ that

preserves densities, is a Markov operator.

Hence, in particular, $P : D \to D$ if P is a Markov operator, and it is straight-forward to check that an FP operator is also a Markov operator.

Of particular interest to us are the Markov operators that can be defined as an integral operator with a stochastic kernel,

$$Pf(x) = \int_X K(x,y)\, f(y)\, \mu(dy) \tag{5}$$

where $K(\cdot,\cdot) : X \times X \to R$ is a measurable function,

$$K(x,y) \geq 0 \tag{6}$$

and

$$\int_X K(x,y)\, \mu(dx) = 1 \tag{7}$$

By invoking Fubini's theorem, it is easily checked that this kind of operator is indeed a Markov operator.

4 THE STOCHASTIC DIFFERENTIAL EQUATION

Throughout, the stochastic differential equations (SDE) will be interpreted in the Itô sense. The class of SDE considered is of the following form

$$dY_t = a(Y_t)\, dt + b(Y_t)\, dW_t \tag{8}$$

where $Y_t = \big(Y_{1,t}, \ldots, Y_{n,t}\big)^T$ = the (n-dimensional) state space vector process, and $W_t = \big(W_{1,t}, \ldots, W_{m,t}\big)^T$ is a standard (unit) scalar or vector (m-dimensional) Brownian motion process [27, 28] depending on the type of system being studied. In the case $m > 1$, it is part of the assumptions that the components of W_t are assumed to be independent. $a(\cdot) = \big(a_1(\cdot), \ldots, a_n(\cdot)\big)^T$ is an (n-dimensional) vector function. Note that $a(Y_t)$ may include Wong-Zakai correction terms if $b(Y_t)$ actually depends on Y_t, and if the SDE models a system driven by wide band processes [27]. $b(\cdot) = \big(b_{ij}(\cdot)\big)$, $i = 1, \ldots, n; j = 1, \ldots, m$ is a vector ($m = 1$) or a matrix function depending on whether W_t is a scalar or vector process.

The methodology we are going to describe in these lecture notes, also applies to the case when the drift term a and the diffusion term b in equation (8)

have explicit time dependence, that is, $a = a(t, Y_t)$ and/or $b = b(t, Y_t)$. However, to simplify the exposition, we have chosen to limit ourselves to the simpler, homogeneous case.

Under sufficient regularity conditions on $a(\cdot)$ and $b(\cdot)$, cf. [28], the solution process Y_t of equation (8) is a Markov process with a.s. continuous paths. This makes it possible to establish a path integration method for the calculation of the (joint) PDF $p(y,t)$ of the solution process Y_t by exploiting the fundamental equation

$$p(y,t) = \int_{-\infty}^{\infty} p(y,t|y',t')\, p(y',t')\, dy' \tag{9}$$

where $p(y,t|y',t')$ denotes the conditional PDF of Y_t given that $Y_{t'} = y'$, and $dy' = dy'_1 \cdots dy'_n$. It is referred to as the transition probability density function (TPD), and it serves as the stochastic kernel of an integral Markov operator. As will be shown, for a numerical solution of an SDE, the TPD can always be given as an analytical, closed form expression. Hence, if an initial PDF, $p_0(y) = p(y, t = 0)$ say, is given, then equation (9) can be invoked repeatedly to produce the time evolution of $p(y,t)$. If the SDE has an invariant measure, that is, there exists a stationary PDF, $p_s(y)$ say, then eventually, assuming that $p_0(y) \neq p_s(y)$, $p(y,t)$ will approach this stationary PDF. The number of times equation (9) has to be repeatedly used to reach the stationary situation, depends, of course, on the dynamic system and on the specified initial PDF $p_0(y)$.

This discussion reveals a fundamental aspect of the PI solution. It is not obtained by numerically solving the Fokker-Planck equation. If this equation has a unique solution, it will invariably agree with the PI solution. However, the theorems on existence and uniqueness of solutions of the FP equation formulated in terms of PDFs put severe restrictions on the nonlinear systems for which solutions are garanteed to exist and be unique. However, as pointed out by [27], these results are believed to fall far short of what is actually true. Whether the PI method can be used to deduce such results is still an open problem.

For a numerical solution of the SDE (8), a discretization procedure has to be adopted. Actually, the SDE (8) is just a short-hand notation for the expression

$$Y_t = Y_{t'} + \int_{t'}^{t} a(Y_s)\, ds + \int_{t'}^{t} b(Y_s)\, dW_s \tag{10}$$

where the last integral is interpreted as an Itô stochastic integral. A numerical solution procedure is then based on choosing a time increment $\Delta t = t - t'$ such

that Y_t can be calculated for each given value of $Y_{t'}$. The basic version is the Euler-Maruyama approximation [30]

$$Y_t = Y_{t'} + a(Y_{t'})\,\Delta t + b(Y_{t'})\,\Delta W_{t'} \tag{11}$$

where $\Delta W_{t'} = W_t - W_{t'}$. Since the Brownian motion process has independent increments, it follows from equation (11) and the definition of $\Delta W_{t'}$, that the sequence $\{\eta_i = Y_{i\Delta t}\}_{i=0}^{\infty}$ is a Markov chain. For sufficiently small Δt, it is assumed that this Markov chain will approximate the continuous time Markov process solution of the SDE (8). It is also observed from equation (11) that the TPD $p(y,t|y',t')$ is a Gaussian PDF since the conditional random variable $(\eta_{i+1}|\eta_i = y') = y' + a(y')\Delta t + b(y')\Delta W_{i\Delta t}$ and $\Delta W_{i\Delta t}$ is a Gaussian variable for every $i = 1, 2, \ldots$.

Considering only the deterministic part of the SDE (8), equation (11) reduces to the Euler approximation $y_t = y_{t'} + a(y_{t'})\,\Delta t$. As is well known, this approximation is only accurate to order $O(\Delta t^2)$. To improve the accuracy of the discretization process in following the evolution in time of the deterministic part of the system, a 4th order Runge-Kutta approximation is implemented, which is accurate to order $O(\Delta t^5)$. This amounts to replacing the function $a(y)$ by the corresponding Runge-Kutta approximation, $r(y)$ say. The explicit expression for $r(y)$ will not be given here since the procedure to obtain it is described in any elementary book on numerical methods. Equation (11) will therefore be replaced by what will be referred to as the Runge-Kutta-Maruyama (RKM) approximation

$$Y_t = Y_{t'} + r(Y_{t'})\,\Delta t + b(Y_{t'})\,\Delta W_{t'} \tag{12}$$

To get the expression for the TPD corresponding to equation (12), we first introduce the diffusion matrix $g(y)$ defined as follows

$$g(y) = \big(g_{ij}(y)\big) = b(y)\,b(y)^T = \Big(\sum_{k=1}^{m} b_{ik}(y) b_{jk}(y)\Big) \tag{13}$$

It is often the case that some of the rows of the matrix $b(y)$ are zero. By reordering, it will be assumed that the first r rows are zero, that is

$$b_{ij}(y) = 0 \qquad \text{for} \quad i = 1, \ldots, r; j = 1, \ldots, m\,(r < n) \tag{14}$$

and that $b_{ij} \neq 0$ for at least one j for every $i = r+1, \ldots, n$. This implies that the diffusion matrix $g(y)$ assumes the form

$$g(y) = \begin{pmatrix} 0 & 0 \\ 0 & \tilde{g}(y) \end{pmatrix} \tag{15}$$

In this matrix 0 denotes appropriate zero-matrices and $\tilde{g}(y)$ denotes an $(n-r)\times(n-r)$-matrix function. It will be assumed that $\tilde{g}(y)$ is a positive definite matrix for all relevant values of y. This leads to the following expression for the TPD

$$\begin{aligned} p(y,t|y',t') = &\prod_{i=1}^{r}\delta(y_i - y_i' - r_i(y')\Delta t) \\ &\cdot \tilde{p}(\tilde{y},t|y',t') \end{aligned} \tag{16}$$

where $\tilde{y} = (y_{r+1},\ldots,y_n)^T$, $\delta(\cdot)$ denotes the Dirac delta function and

$$\begin{aligned} \tilde{p}(\tilde{y},t|y',t') = &\frac{1}{(2\pi\,\Delta t)^{(n-r)/2}}|\tilde{g}(y')|^{-1/2}\cdot\exp\Big\{-\frac{1}{2\,\Delta t}\sum_{i=r+1}^{n}\sum_{j=r+1}^{n} \\ &\big(y_i - y_i' - r_i(y')\,\Delta t\big)\,[\tilde{g}(y')^{-1}]_{i-r,j-r}\,\big(y_j - y_j' - r_j(y')\,\Delta t\big)\Big\} \end{aligned} \tag{17}$$

where $|\tilde{g}|$ denotes the determinant of the reduced diffusion matrix $\tilde{g}$, assumed to be positive definite. This implies that $|\tilde{g}| > 0$. $[\tilde{g}(y')^{-1}]_{ij}$ denotes the element in position ij of the inverse matrix of $\tilde{g}$. Hence, if $r > 0$, $p(y,t|y',t')$ is a degenerate multidimensional Gaussian PDF.

Thus, for the RKM approximation to the SDE, we have shown that an explicit expression for the TPD is at hand. As already pointed out, equation (9) therefore provides a vehicle for numerical solution of the SDE through iterated calculation of the PDF of the state space vector associated with the approximating Markov chain $\{\eta_i\}$.

It is realized that in the RKM approximation, the simplest approximation to the integral $\int_{t'}^{t} b(Y_s)dW_s$ is still retained. Improved approximations to this integral can be taken into account in some cases as discussed in [13, 29]. However, the experience has been that to improve numerical efficiency, relatively little is gained such improvements. The the most important modification to implement in the computer code appears to be the Runge-Kutta approximation to the deterministic part of the SDE.

It is recognized that the numerical schemes used throughout the present work are explicit forward time stepping methods, and in general such methods are only conditionally stable. For a more thorough discussion of such matters, the reader is referred to [30], which provides an extensive coverage of convergence and stability properties of various explicit and implicit numerical schemes relating to SDEs.

5 GENERALIZED CELL MAPPING

We have seen in the previous section that the TPD $p(y,t|y',t')$ can be given explicitly and in closed form for the discretized SDE whether it be given by

equation (11) or (12). This makes possible the numerical implementation of the PIS.

GCM [31] is the natural first approach at implementing numerical diffusion of probability as expressed by equation (9). The GCM is based on dividing the state space into a suitable number of nonoverlapping cells. The cells may be of equal size for simplicity, which is produced by equidistant discretizations of the relevant parts of the state space coordinate axes, or of different size for computational efficiency reasons.

Assuming that the state space vector has dimension n, and that the number of discretization intervals along coordinate axis no. i is equal to l_i, then the total number of cells will be $l = l_1 \times \ldots \times l_n$. For each cell no. j, $j = 1, \ldots, l$, there is at time $t = t_i$, $i = 0, 1, 2, \ldots$ associated a probability mass $\pi_j^{(i)}$. The corresponding approximation to equation (9) can then be written as

$$\pi_k^{(i)} = \sum_{j=1}^{l} P_{kj}^{(i,i-1)} \, \pi_j^{(i-1)} \tag{18}$$

where $P_{kj}^{(i,i-1)}$ denotes the $l \times l$ transition probability matrix (TPM) from $t = t_{i-1}$ to $t = t_i$ of the l-dimensional Markov chain resulting from the division of state space into l cells. Hence, as formulated in [32]: "The fundamental unit operation in this approach is the diffusion of probability mass in one cell at time t_{i-1} into a number of neighbouring cells at time t_i". This is illustrated in Figure 2. The probability mass marked with gray in Figure 2a is distributed according to equation (18) into other cells as shown in Figure 2b. By performing the same procedure for all the PDF parts of Figure 2a and adding together the probability masses over one cell, the PDF at time t_i is obtained, cf. equation (18).

The evolution with time of the probability mass vector $\pi_j^{(i)}$ is then found by repeating the operation of equation (18) the required number of times. It is recognized that to retain a certain accuracy in the calculation of the probability mass vector as time evolves, requirements have to be put on both the cell size and the time increment, and also on a balance between these two factors. Simply stated, small time steps require small cell size.

An alternative approach was investigated by Sun & Hsu [9]. They introduced the assumption that the TPD associated with equation (10) for a suitably short time increment was a non-degenerate Gaussian PDF. By appropriate assumptions, a set of moment equations for this TPD was established. Solving these equations then provided the requisite TPM for obtaining an approximate solution by the GCM method. They showed that this technique allowed for fairly big time steps and thereby reasonable cell size.

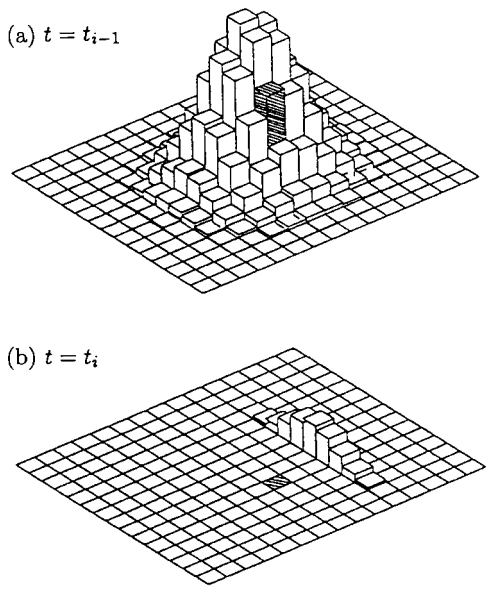

Figure 2: Illustration of the GCM scheme.

6 NUMERICAL IMPLEMENTATION OF PATH INTEGRATION

Let us take a closer look at equation (9). It is realized from equations (16) and (17) that the TPD is highly localized in state space for small values of Δt. Hence, to obtain an accurate result for $p(y,t)$ by using equation (9), an accurate representation of $p(y',t')$ is required. This can be achieved by using a very fine mesh in the whole domain where $p(y',t')$ is calculated for every grid point of the mesh, as in the GCM method. However, this quickly leads to excessive CPU times when the dimension of the problem increases.

A better approach is to use a coarse mesh in combination with an interpolation procedure [10, 11]. Here we shall focus on using splines to represent $p(y',t')$, specifically cubic B-splines [33]. Hence, at each time step $t' \rightarrow t$, $p(y',t')$ is represented as a cubic B-splines series in the following manner

$$p(y',t') = \sum_{k_1=1}^{M_1} \cdots \sum_{k_n=1}^{M_n} \Gamma_{t'}(k_1,\ldots,k_n) \bigotimes_{i=1}^{n} B_{k_i}(y') \tag{19}$$

where M_j = number of grid points for the i'th state variable y_i, $\{\otimes_{i=1}^{n} B_{k_i}(\cdot)\}_{k_i=1}^{M_i}$ is a tensor product basis of cubic B-splines [33] and $\{\Gamma_{t'}(k_1,\ldots,k_n)\}_{k_i=1}^{M_i}$ is the set of interpolation coefficients associated with time t'. It is assumed that each

set $\{B_{k_i}(\cdot)\}_{k_i=1}^{M_i}, i = 1, \ldots, n$, is a basis of cubic B-splines associated with the knot sequence [33] determined by the grid points for the i'th variable y_i. The tensor product B-spline $\otimes_{i=1}^{n} B_{k_i} : R^n \to R$, where $R = (-\infty, \infty)$, is defined by

$$\bigotimes_{i=1}^{n} B_{k_i}(y) = \prod_{i=1}^{n} B_{k_i}(y_i) \tag{20}$$

The representation of $p(y', t')$ by B-splines makes it possible to retain high numerical accuracy even with a fairly coarse basic grid if $p(y', t')$ is not too singular. By substituting from equation (19) into equation (9), it is obtained that

$$\begin{aligned} p(y,t) = & \sum_{k_1=1}^{M_1} \cdots \sum_{k_n=1}^{M_n} \Gamma_{t'}(k_1, \ldots, k_n) \\ & \cdot \int_{D_1} \cdots \int_{D_n} p(y,t|y',t') \bigotimes_{i=1}^{n} B_{k_i}(y')\, dy' \end{aligned} \tag{21}$$

where D_i denotes the integration domain for y_i', $i = 1, \ldots, n$. Note that the first r integrals are only formal integrals due to the delta-function behaviour of the TPD, cf. equation (16). We shall return to this point later.

We have made the assumption that the drift term a and the diffusion term b in equation (8) do not explicitly depend on the time parameter t, that is, the Markov process Y_t will be (time-)homogeneous. It follows from equation (19) that

$$p(y,t|y',t') = p(y, \Delta t|y', 0) \tag{22}$$

Hence, from equation (21) it is seen that for a fixed value of the time increment Δt, each of the integrals on the right hand side of this equation need to be calculated only once, and can be stored for repeated use. That is, the following parameters may be calculated initially and stored

$$B_{l_1 \ldots l_n}^{k_1 \ldots k_n} = \int_{D_1} \cdots \int_{D_n} p(y_{(l_1 \ldots l_n)}, \Delta t|y', 0) \bigotimes_{i=1}^{n} B_{k_i}(y')\, dy' \tag{23}$$

Here the index l_i, $i = 1, \ldots, n$, refers to grid point number l_i for the state space variable y_i. It may be noted that due to the properties of the TPD for small time increments Δt, the tensor $B_{l_1 \ldots l_n}^{k_1 \ldots k_n}$ has a strongly banded character with the elements decreasing rapidly away from the main diagonal $k_1 = l_1, \ldots, k_n = l_n$. This has important implications for the efficiency of computer programs designed to use PI to solve SDEs. Combining equations (21) and (23) gives

$$p(y_{(l_1 \ldots l_n)}, t) = \sum_{k_1=1}^{M_1} \cdots \sum_{k_n=1}^{M_n} \Gamma_{t'}(k_1, \ldots, k_n)\, B_{l_1 \ldots l_n}^{k_1 \ldots k_n} \tag{24}$$

What needs to be calculated at each time step $t' \rightarrow t$ is then the interpolation coefficients $\Gamma_{t'}(k_1, \ldots, k_n)$.

The interpolation procedure described above in general requires a rather fine mesh in the tail regions of the PDF to achieve the necessary precision. The reason for this is not hard to understand. By their very construction, splines are expectedly best at reproducing polynomials and polynomial-like functions. Considering that for large classes of problems, $\ln[p(y', t')]$ is in fact quite close to a polynomial function, Naess & Moe [13, 29] adopted the strategy of a splines representation of $\ln[p(y', t')]$ instead of $p(y', t')$ itself. Another representation strategy has been investigated by Yu et al. [12].

Specifically, the following representation as a pp-form series based on cubic splines [33] was adopted

$$\begin{aligned} -\ln[p(y', t')] = & \sum_{k_1=1}^{M_1-3} \cdots \sum_{k_n=1}^{M_n-3} I_{k_1,\ldots,k_n}(y') \\ & \cdot \sum_{l_1=0}^{3} \cdots \sum_{l_n=0}^{3} \gamma_{l_1,\ldots,l_n}^{k_1,\ldots,k_n} \cdot (y_1')^{l_1} \cdot \ldots \cdot (y_n')^{l_n} \end{aligned} \tag{25}$$

M_i = number of grid points for the i'th state space variable y_i. In our case, there are $M_i - 3$ intervals I_{k_i} on the y_i-axis relative to which the cubic splines are defined. This is related to the choice of knot sequence [33]. The function $I_{k_1,\ldots,k_n}(y') = 1$ if y' belongs to the subdomain given by the Cartesian product $I_{k_1} \times \ldots \times I_{k_n}$, while it is equal to zero if y' does not belong to this subdomain. For each subdomain, uniquely specified by the indices $k_1, \ldots, k_n$, the coefficients $\gamma_{l_1,\ldots,l_n}^{k_1,\ldots,k_n} = \gamma_{l_1,\ldots,l_n}^{k_1,\ldots,k_n}(t')$ of the pp-form splines representation are determined by adapting algorithms given by de Boor [33].

The expression analogous to equation (21) is for this case

$$\begin{aligned} p(y, t) = \int_{D_1} \cdots \int_{D_n} p(y, t|y', t') \cdot \exp\Big\{ & -\sum_{k_1=1}^{M_1-3} \cdots \sum_{k_n=1}^{M_n-3} I_{k_1,\ldots,k_n}(y') \\ & \cdot \sum_{l_1=0}^{3} \cdots \sum_{l_n=0}^{3} \gamma_{l_1,\ldots,l_n}^{k_1,\ldots,k_n} \cdot (y_1')^{l_1} \cdot \ldots \cdot (y_n')^{l_n} \Big\}\, dy' \end{aligned} \tag{26}$$

It is recognized that for this formulation of the interpolation procedure, there is no formula corresponding to equation (24). That is, the integrations of

equation (26) have to be carried out at each time step. Hence the potential gain in CPU time achieved by a coarser grid for this formulation is to some extent lost by these repeated integrations. On the other hand, there is no added cost to treat the case of explicit time dependence of the drift and diffusion terms in the SDE.

A point to observe at this stage is the fact that $p(y,t)$ in equations (21) and (26) is calculated only for the points of the chosen grid, that is, for $y = y_{(l_1 \ldots l_n)}$. This has the implication that the numerical evaluation of the integral of equations (21) or (26) in fact should be based on a backward time-stepping procedure, as opposed to the GCM, which is a purely forward time-stepping method. Figure 3 illustrates how the backward time-stepping is implemented. The point y' is determined by following the deterministic path backwards from y for the time duration Δt. The points $y'_A = (y'_{1A}, \ldots, y'_{nA})^T$ and $y'_B = (y'_{1B}, \ldots, y'_{nB})^T$, which give the integration limits in equation (21) or (26), that is, $D_i = (y'_{iA}, y'_{iB})$, are determined by backward time-stepping of the corresponding points y_A and y_B, requiring that (the non-degenerate part of) the TPD functions centered at y_A and y_B assume values less than a preassigned threshold value at the point y, typically 10^{-6}. The choice of threshold value will depend on the grid mesh. The chosen value should be small enough to ensure that the probability of a point starting at e.g. y'_A to end up at y after one (forward) time step is sufficiently small.

This backward time stepping procedure is of considerable computational advantage in the sense that it allows a relatively coarse grid. With the calculation procedure adopted here, the density of grid points is solely determined by the ability to represent the PDF at each time step by e.g. a splines approximation in a sufficiently accurate manner. What is sufficiently accurate, is to some extent problem specific. A more detailed discussion of the numerical aspects of the proposed implementation is given in Moe [34]. Figure 4 illustrates the numerical PI scheme

To ensure a correct normalization, checks on the value of the integral $\int p(y,t)\,dy$ have to be made repeatedly after a suitable number of iterations. If the calculated value deviates from 1.0 relative to a preassigned accuracy, the coefficients of the splines representation are updated accordingly.

Let us now return to the previous comment that the first r integrals in equations (21) and (26) are only formal integrals. At the same time we want to point out one of the significant advantages of numerical PI for solving an important class of SDEs obtained from nonlinear dynamic systems. Very often the stochastic excitation only enters through one of the dimensions of the state space vector, that is, $r = n - 1$. Under this assumption, it is recognized that the integrations of equations (21) and (26) in fact reduces to an integration of only one variable, viz. y'_n. This follows by observing that for $1 \leq i \leq n-1$, due to the degenerate form of the TPD, cf. equation (16), the integration variable y'_i is obtained as a function of $y = (y_1, \ldots, y_n)^T$ and y'_n by solving the set of

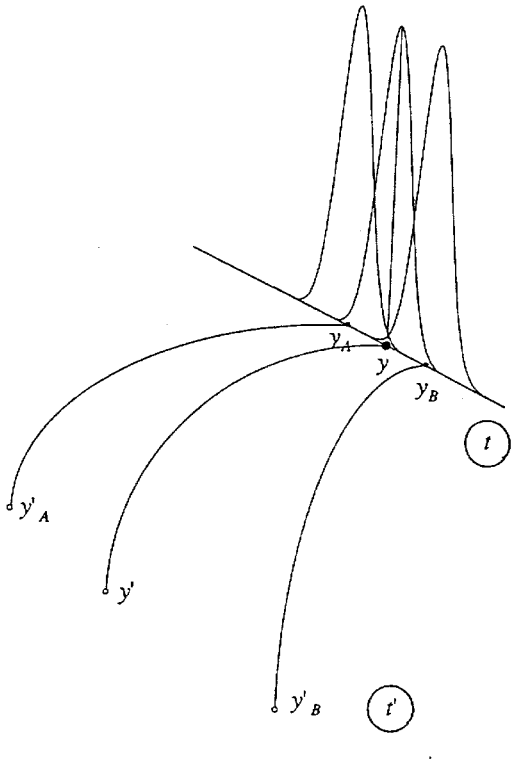

Figure 3: Illustration of the backward time-stepping procedure.

equations $y_i = y'_i + r_i(y')\Delta t$. A first approximation is obviously obtained by setting $y'_i = y_i - r_i(y)\Delta t$, which can be sharpened by iteration in an obvious manner. Denote the solutions by $\tilde{y}'_i = \psi_i(y'_n; y)$, and $\tilde{y}' = (\tilde{y}'_1, \ldots, \tilde{y}'_{n-1}, y'_n)^T$. Then equation (21) assumes the form

$$p(y,t) = \sum_{k_1=1}^{M_1} \cdots \sum_{k_n=1}^{M_n} \Gamma_{t'}(k_1, \ldots, k_n) \cdot \int_{y'_{nA}}^{y'_{nB}} \tilde{p}(y_n, t|\tilde{y}', t') \bigotimes_{i=1}^{n} B_{k_i}(\tilde{y}')\, dy'_n \tag{27}$$

so that the calculation of the coefficients $B_{l_1 \ldots l_n}^{k_1 \ldots k_n}$ in equation (23) only involves a one-dimensional integration.

In the same manner, equation (26) can be written in the following form

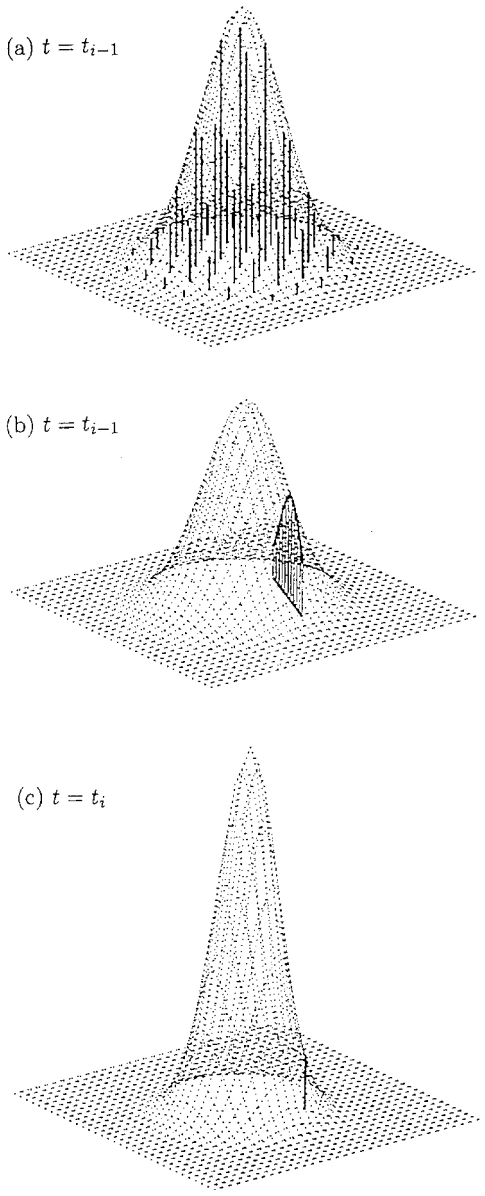

Figure 4: Pictorial representation of the PI scheme.

$$p(y,t) = \int_{y'_{nA}}^{y'_{nB}} \tilde{p}(y_n, t|\tilde{y}', t') \cdot \exp\left\{ - \sum_{k_1=1}^{M_1-3} \cdots \sum_{k_n=1}^{M_n-3} I_{k_1,\ldots,k_n}(\tilde{y}') \right.$$
$$\left. \cdot \sum_{l_1=0}^{3} \cdots \sum_{l_n=0}^{3} \gamma_{l_1,\ldots,l_n}^{k_1,\ldots,k_n} \cdot (\tilde{y}'_1)^{l_1} \cdot \ldots \cdot (\tilde{y}'_{n-1})^{l_{n-1}} \cdot (y'_n)^{l_n} \right\} dy'_n \tag{28}$$

The number of integrations that has to be carried out in equations (21) and (26) have significant implications for the CPU time needed to solve a specific problem. Hence it is of great advantage when the required integrations can be reduced to only one, as above. Clearly, in general, this cannot be done. Note that the positivity of the calculated PDF $p(y,t)$ is guaranteed by the fact that both functions entering the integration on the rhs of equation (11) are invariably non-negative.

We close this section by a discussion of a technique for complexity reduction which is often useful. For many dynamic models not all state space dimensions are of equal interest. In fact, very often it is only the first two state space dimensions that are of immediate interest, but the remaining dimensions are needed to obtain a SDE. In such cases one might consider simplifying the numerical calculations by retaining an accurate representation in term of splines only for the first two dimensions while treating the remaining dimensions only as slave variables with a coarse numerical representation. However, practical experience has shown that to obtain accurate results for the first two dimensions, there appears to be a rather stringent requirement regarding representation accuracy also for the slave variables.

Let us illustrate one such possible approach for the 4D situation. Assuming that the PDF $p(y)$ of the state space vector Y_t has been calculated for the points of the chosen grid, which are here generically denoted by $(y_{1k}, y_{2l}, y_{3m}, y_{4n})$. For each point (y_{3m}, y_{4n}), a splines representation $p_{mn}(y_1, y_2)$ can be calculated for the first two state space dimensions. When $y_{3m} < y_3 < y_{3m+1}$ and $y_{4n} < y_4 < y_{4n+1}$, a 4D interpolation for $p(y)$ is then calculated by the expression

$$\begin{aligned} p(y) &= (1-\lambda_m)(1-\lambda_n)p_{mn}(y_1,y_2) \\ &+ \lambda_m(1-\lambda_n)p_{m+1n}(y_1,y_2) \\ &+ (1-\lambda_m)\lambda_n p_{mn+1}(y_1,y_2) \\ &+ \lambda_m\lambda_n p_{m+1n+1}(y_1,y_2) \end{aligned} \tag{29}$$

where

$$\lambda_m = \frac{y_3 - y_{3m}}{y_{3m+1} - y_{3m}} \tag{30}$$

$$\lambda_n = \frac{y_4 - y_{4n}}{y_{4n+1} - y_{4n}}. \tag{31}$$

This simple procedure has been used to calculate the stationary PDF of some nonlinear oscillators leading to 4D SDEs, as will be shown in the next section.

7 NUMERICAL EXAMPLES

The performance of the numerical PI procedure described in these notes will be illustrated by application to a few special cases of some classes of nonlinear oscillators driven by white or coloured noise. In this section we shall refer to the two basic methods of splines interpolation presented in the previous section as Splines A (for $p(y,t)$) and Splines B (for $\ln[p(y,t)]$).

CLASS 1 - Nonlinear oscillators with additive noise

The first type of oscillators within this class are characterized by the dynamic model, cf. [35],

$$\ddot{X}_t + g(E)\,\dot{X}_t + h(X_t) = F_t \tag{32}$$

where $g(\cdot)$ and $h(\cdot)$ are suitable functions. $E = E(X_t, \dot{X}_t)$ denotes the total energy, that is

$$E = \frac{1}{2}\,\dot{X}_t^2 + V(X_t) \tag{33}$$

where the potential energy function $V(\cdot)$ is given by the relation

$$V(x) = \int_0^x h(s)\,ds \tag{34}$$

The external excitation process F_t of equation (29) will be chosen first as a stationary Gaussian white noise, which means that equation (29) corresponds to a 2D SDE ($n = 2$, $m = 1$, cf. equation (8)), where $Y_t = (Y_{1,t}, Y_{2,t})^T = (X_t, \dot{X}_t)^T$, $a(Y_t) = \big(Y_{2t}, -g(E)Y_{2t} - h(Y_{1t})\big)^T$, and $b(Y_t) = \big(0, \gamma\big)^T$, and γ is a positive constant.

It can be shown that the stationary joint PDF $p_s(y_1, y_2)$ determined by equation (32) for this case is given by the formula [35]

$$p_s(y_1, y_2) = C\,\exp\Big\{-\frac{2}{\gamma^2}\int_0^{E(y_1,y_2)} g(s)\,ds\Big\} \tag{35}$$

where C = normalization constant.

This case will be illustrated by the following two examples.

Example 1 - Duffing I

The classical Duffing oscillator (in normalized form) is obtained by setting $g(E) = 2\,\xi$, where ξ is some positive constant, and $h(X_t) = X_t + \lambda\, X_t^3$. By choosing $\gamma = 2\,\sqrt{\xi}$, it follows that for this case

$$p_s(y_1, y_2) = C\, \exp\Big\{ -\frac{1}{2}\big(y_1^2 + \frac{\lambda}{2} y_1^4 + y_2^2\big) \Big\} \tag{36}$$

Note that the parameter ξ does not appear in the expression for p_s, which is due to the specific choice of γ. For the numerical calculations, $\xi = 0.25$ and $\lambda = 0.2$ and 1.0.

Numerical results obtained for the stationary PDF using Splines A combined with a 31×31 grid, starting from an initial Gaussian PDF with zero mean, are plotted in the form of marginal displacement PDFs in Figure 5. For comparison also the corresponding analytical results have been drawn. The agreement is seen to be excellent.

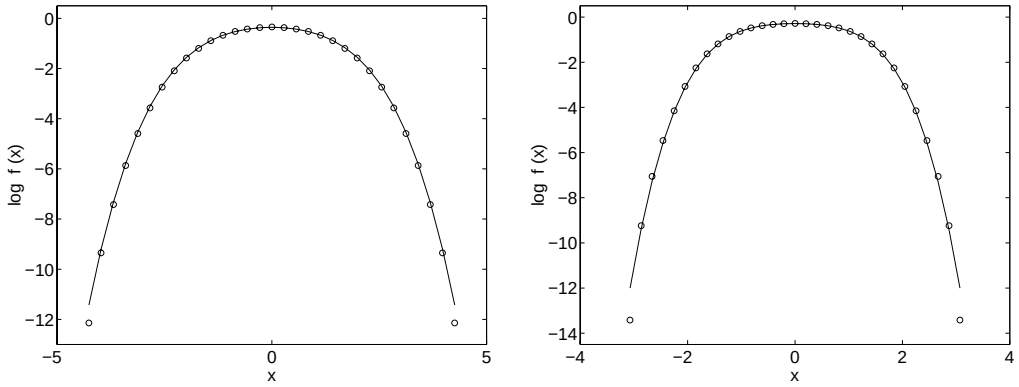

Figure 5: Logarithmic plots of exact (solid line) vs. numerical PI ($\circ\ \circ\ \circ$) results using Splines A for the marginal stationary displacement response PDF of the 2D Duffing oscillator. Left figure: $\lambda = 0.2$. Right figure: $\lambda = 1.0$

Analogously, in Figure 6 are shown numerical results obtained by using Splines B for a 23×23-grid and an initial Gaussian PDF with mean value zero. The corresponding analytical results are also shown. The results are presented in the form of the marginal stationary PDFs for displacement and velocity. It is seen that the agreement is very good down to extremely low probability levels, except for a slight overshoot in the central part of the marginal PDF of the displacement response.

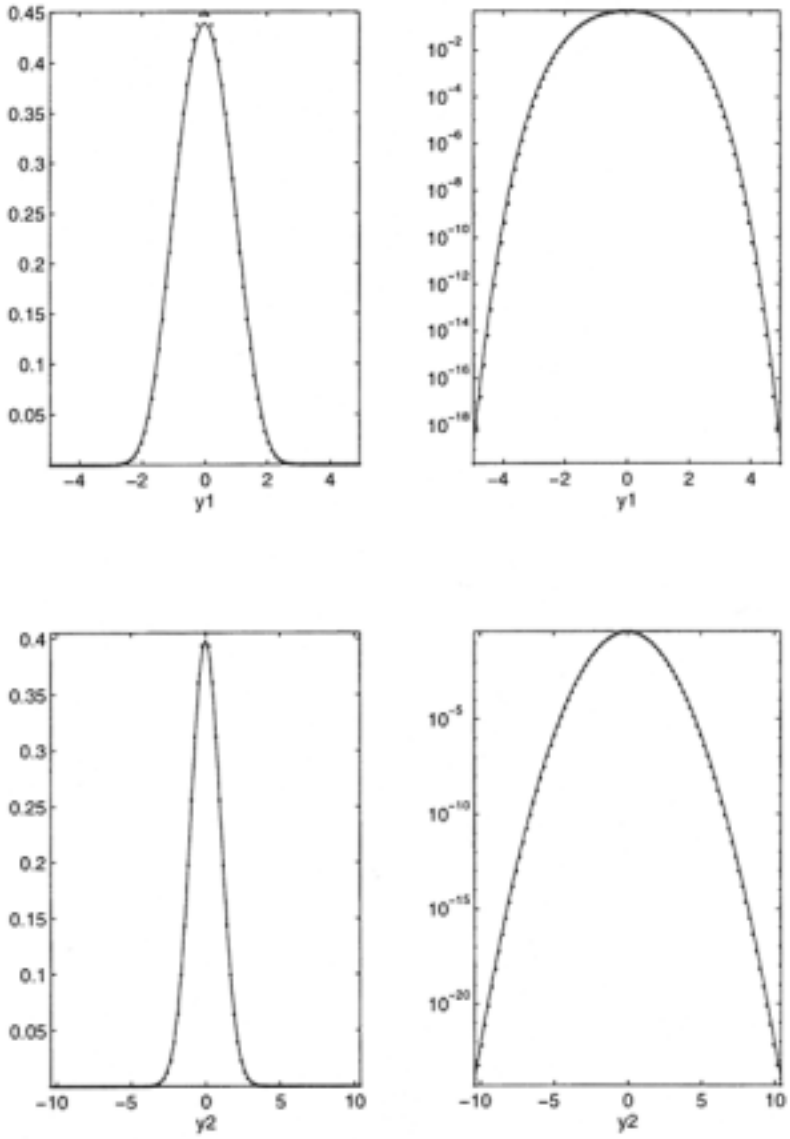

Figure 6: Linear and logarithmic plots of exact (solid line) vs. numerical PI (• • •) results using Splines B for the marginal stationary response PDF of the 2D Duffing oscillator (Example 1) for $\lambda = 0.2$. Top figures: Displacement. Bottom figures: Velocity

Example 2 - Duffing II

This example distinguishes itself from Example 1 only by the way the function h is chosen. Here $h(X_t) = -X_t + \lambda X_t^3$, corresponding to what is often called a double potential well. In this case

$$p_s(y_1, y_2) = C \, \exp\Big\{ \, -\frac{1}{2}\Big(\, - \, y_1^2 + \frac{\lambda}{2} y_1^4 + y_2^2\Big) \, \Big\} \tag{37}$$

which is recognized as a two-peaked PDF.

It is seen from Figure 7 that the results obtained by numerical PI using Splines B based on a 15×15-grid and an initial Gaussian PDF with mean value zero, compares well with the analytical results.

The next type of nonlinear system with additive noise that we shall work with, is the Duffing - van der Pol Oscillator. The equation of motion for this oscillator is as follows

$$\ddot{X}_t + 2\,\zeta\,(X_t^2 - 1)\,\dot{X}_t + X_t + \lambda\, X_t^3 = F_t \tag{38}$$

where ζ is a positive constant.

Example 3 - Van der Pol oscillator

This case is obtained by putting $\lambda = 0$. We shall in this example consider a van der Pol oscillator driven by stationary Gaussian white noise. Similarly to the two preceding examples, this leads to a 2D SDE. This example has been calculated using only Splines A with a 41×41 grid. Since no closed form expression is known for the stationary PDF for this case, Monte Carlo simulations were carried out to get an empirical estimate of the PDF for the purpose of comparison. To get good empirical estimates down to the 10^{-7} level, about 12 hours of CPU time was needed on the work station used. In contrast, the PI solution takes a few seconds, which is essentially the same for all 2D problems.

The numerical results for two specific choices of ζ-values, have been presented in Figures 8 and 9 in the form of marginal PDFs. Figure 10 shows 3D plots of the corresponding joint PDFs.

In the next two examples, we shall consider additive coloured noise obtained by passing Gaussian white noise through a second order linear filter. Specifically, the coloured noise F_t is determined by the equation

$$\ddot{F}_t + 2\,\kappa\,\omega_s\,\dot{F}_t + \omega_s^2\,F_t = \alpha\,N_t \tag{39}$$

where α, κ and ω_s are positive constants, and $N(t)$ denotes (symbolically) standard Gaussian white noise. This means that F_t satisfies a 2D linear SDE,

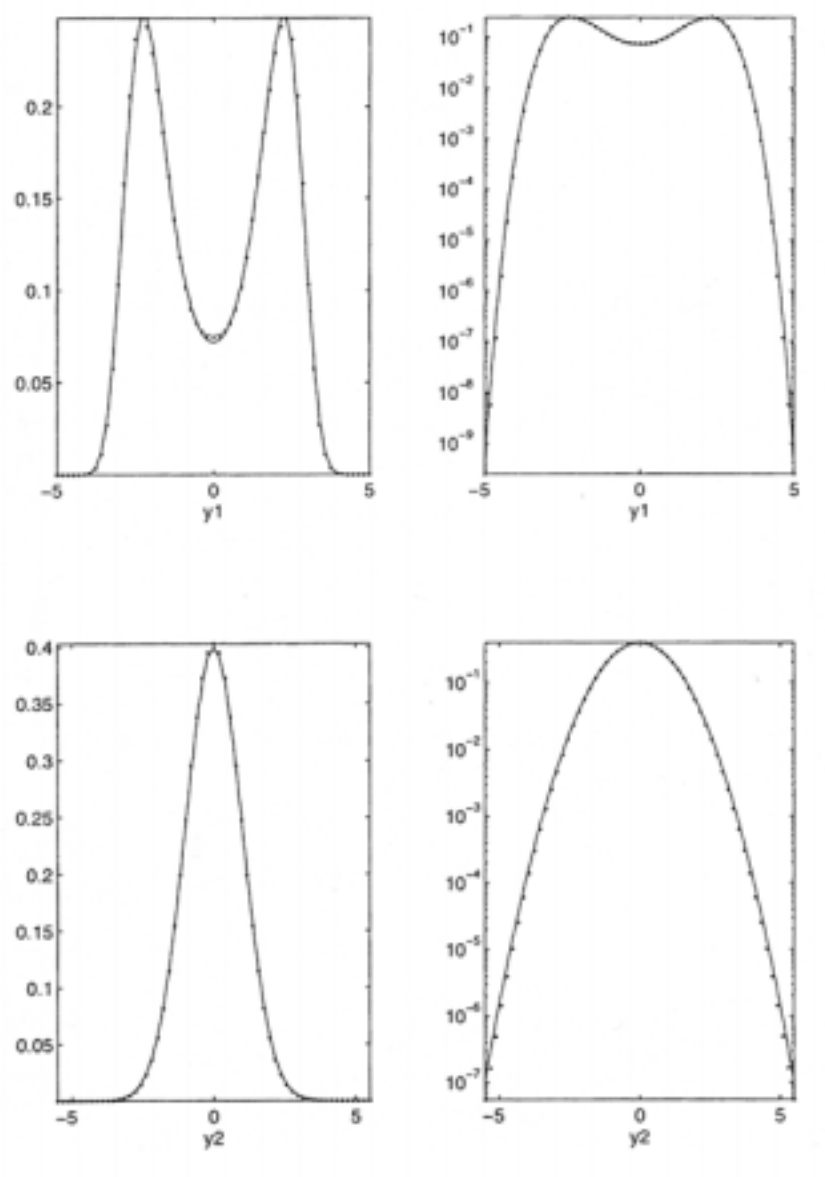

Figure 7: Linear and logarithmic plots of exact (solid line) vs. numerical PI ((• • •) results using Splines B for the marginal stationary response PDF of the 2D Duffing oscillator (Example 2) for $\lambda = 0.2$. Top figures: Displacement. Bottom figures: Velocity

and it follows that F_t becomes a stationary Gaussian process with zero mean and spectral density given by the expression

$$S(\omega) = \frac{\alpha^2}{2\,\pi[(\omega^2 - \omega_s^2)^2 - (2\kappa\omega_s\omega)^2]} \tag{40}$$

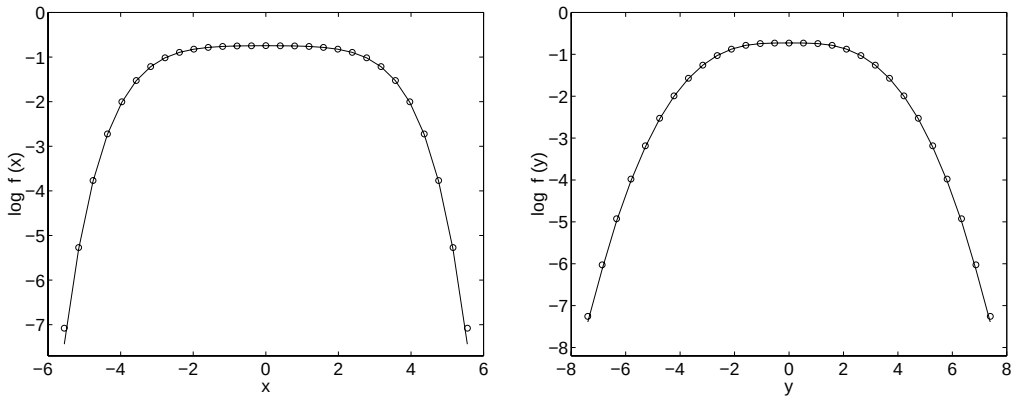

Figure 8: Logarithmic plot of Monte Carlo (solid line) vs. numerical PI ($\circ\ \circ\ \circ$) results for the marginal stationary response PDF of the van der Pol oscillator for $\zeta = 0.05$. Left figure: Displacement. Right figure: Velocity

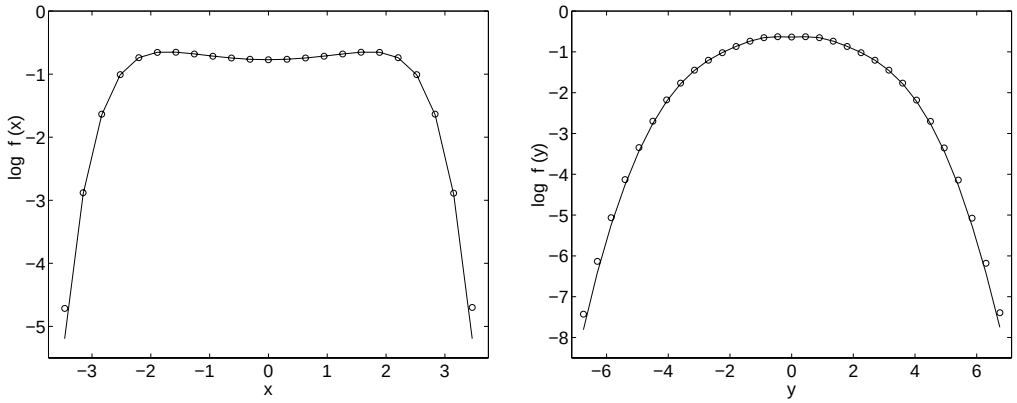

Figure 9: Logarithmic plot of Monte Carlo (solid line) vs. numerical PI ($\circ\ \circ\ \circ$) results for the marginal stationary response PDF of the van der Pol oscillator for $\zeta = 0.25$. Left figure: Displacement. Right figure: Velocity

This spectral density has been drawn in Figure 11 for $\alpha = \omega_s = 1.0$ and $\kappa = 0.02$, which are the values to be used in the next two examples. In the figure is also shown a part of a realization of the corresponding F_t. It is seen that this coloured noise is indeed very narrow band in character, as opposed to a white noise.

Example 4 - 4D Duffing

It is recognized that the Duffing oscillator driven by the coloured noise given above leads to a 4D SDE where $Y_t = (Y_{1,t}, Y_{2,t}, Y_{3,t}, Y_{4,t})^T = \left(X_t, \dot{X}_t, F_t, \dot{F}_t\right)^T$, $a(Y_t) = \left(Y_{2,t}, -2\,\xi\,Y_{2,t} - Y_{1,t} - \lambda Y_{1,t}^3 + Y_{3,t}, Y_{4,t},\ -2\,\kappa\,\omega_s\,Y_{4,t} - \omega_s^2\,Y_{3,t}\right)^T$, and

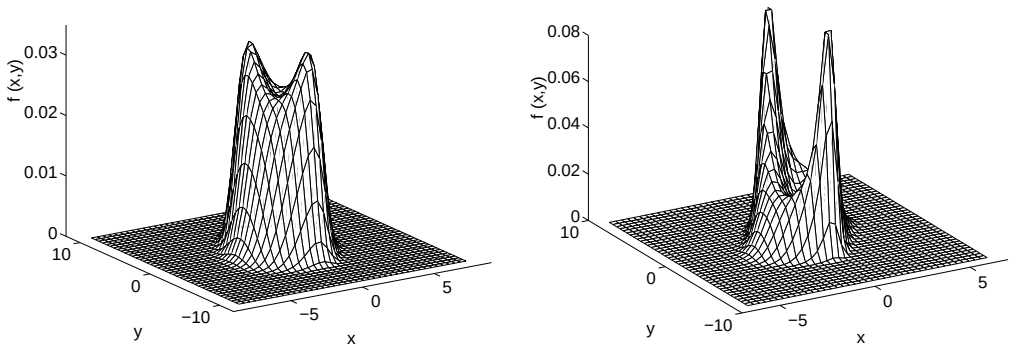

Figure 10: 3D plot of numerical PI results for the joint stationary response PDF of the van der Pol oscillator. Left figure: $\zeta = 0.05$. Right figure: $\zeta = 0.25$.

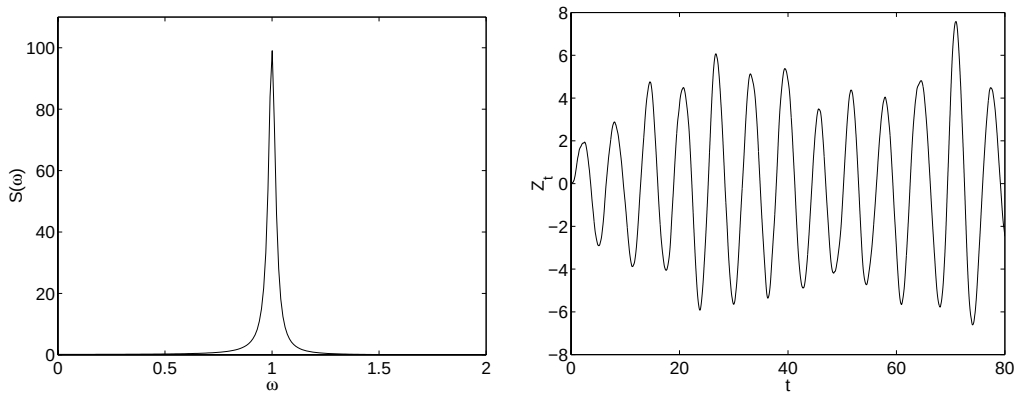

Figure 11: Left figure: Plot of the spectral density of the coloured noise F_t for $\alpha = \omega_s = 1.0$ and $\kappa = 0.02$. Right figure: Part of a realization of F_t.

$b(Y_t) = \big(0, 0, 0, \alpha\big)^T$.

For the numerical calculations Splines A was used for the first two dimensions, while linear interpolation as described in the previous section was applied for the remaining two. The grid was 41^4. Again, for comparison, an empirical PDF was established by Monte Carlo simulations, which required about 24 hours on the work station used for the calculations. In this case the PI solution took about 30 minutes.

The numerical results for $\lambda = 1.0$ have been presented in Figure 12 in the form of marginal stationary PDFs. Note that the marginal velocity distribution is distinctly non-Gaussian in this case as opposed to the white noise driven oscillator, when it is always Gaussian.

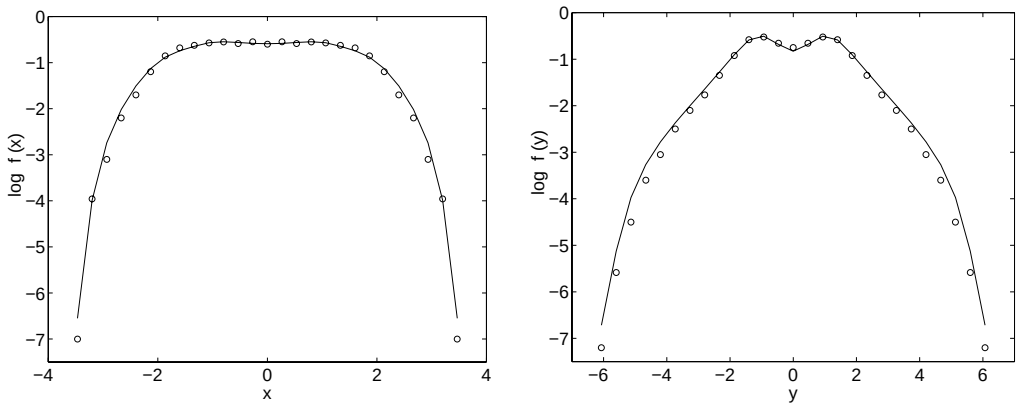

Figure 12: Logarithmic plot of Monte Carlo (solid line) vs. numerical PI ($\circ$ $\circ$ $\circ$) results for the marginal stationary response PDF of the 4D Duffing oscillator for $\lambda = 1.0$. Left figure: Displacement. Right figure: Velocity

Example 5 - 4D Duffing - van der Pol

Let us now look at the Duffing - van der Pol oscillator driven by the coloured noise F_t. The specifics are the same as for Example 4, and we put $\lambda = \zeta = 1$. The results obtained are shown in Figure 13.

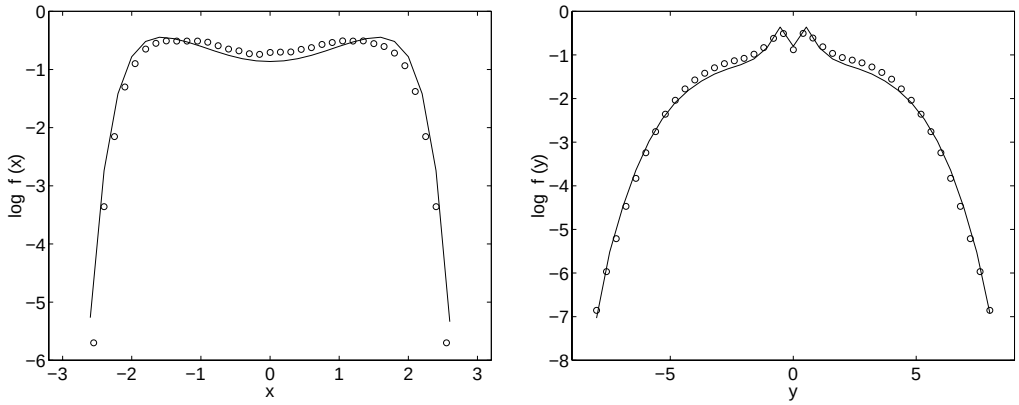

Figure 13: Logarithmic plot of Monte Carlo (solid line) vs. numerical PI ($\circ$ $\circ$ $\circ$) results for the marginal stationary response PDF of the 4D Duffing - van der Pol oscillator for $\lambda = \zeta = 1.0$. Left figure: Displacement. Right figure: Velocity

It is seen that the agreement between the Monte Carlo and the PI results are fairly good, but not on the same level as for the previous example. This can be better understood by looking at the 3D plots of the two joint PDFs, which are given in Figure 14.

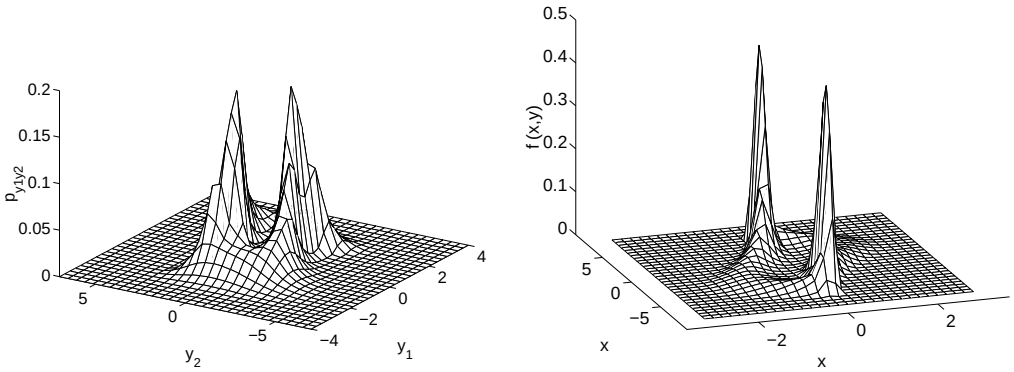

Figure 14: 3D plot of numerical PI results for the joint stationary response PDF of displacement and velocity of oscillator. Left figure: 4D Duffing. Right figure: 4D Duffing - van der Pol.

CLASS 2 - Nonlinear Oscillators with Parametric Excitation

This case is concerned with a class of parametrically excited nonlinear oscillators with equation of motion of the form

$$\begin{aligned} \ddot{X}_t + 2\alpha\dot{X}_t\left(1+\gamma_1 N_{1,t}\right) + \beta\dot{X}_t\left(X_t^2 + \dot{X}_t{}^2/\omega^2\right) \\ + \omega^2 X_t\left(1+\gamma_2 N_{2,t}\right) = \gamma_3 N_{3,t} \end{aligned} \tag{41}$$

Here α, β and ω are positive constants. The stationary Gaussian white noise processes $N_{i,t}$, $i = 1,2,3$, are independent and satisfy the same condition as N_t above. The parameters γ_i, $i = 1,2,3$, represent the intensities of the excitations.

Dimentberg [36] has shown that when

$$\omega^2\gamma_2^2 = 4\alpha^2\gamma_1^2 \tag{42}$$

the stationary PDF exists and is given by the expression

$$p_s(y_1,y_2) = C\left(\kappa + y_1^2 + y_2^2/\omega^2\right)^{\kappa\mu-\delta}\exp\left\{-\mu\left(y_1^2 + \frac{y_2^2}{\omega^2}\right)\right\} \tag{43}$$

where C is a normalization constant, and

$$\kappa = \frac{\gamma_3^2}{\gamma_2^2\omega^4}, \quad \delta = \frac{2\alpha}{\gamma_2^2\omega^2} + \frac{1}{2}, \quad \mu = \frac{\beta}{\gamma_2^2\omega^2} \tag{44}$$

Here we shall present results for the stationary PDF of two specific examples where a closed form solution is known for the first example, but is unknown for the second. The results obtained by the PI method are therefore

compared with results obtained by Monte Carlo simulation for the last example. The PI results are in both examples calculated using Splines B on the basis of an equidistant 25×25-grid for the chosen calculation domain and an initial Gaussian density with mean value zero.

In each case a 2D SDE ($n = 2, m = 3$) is obtained, where $Y_t = (Y_{1,t}, Y_{2,t})^T = (X_t, \dot{X}_t)^T$, $a(Y_t) = (a_1(Y_t), a_2(Y_t))^T = (Y_{2,t}, -2\alpha Y_{2,t} - \beta Y_{2,t}(Y_{1,t}^2 + Y_{2,t}/\omega^2) - \omega^2 Y_{1,t} + 2\alpha^2\chi_1^2 Y_{2,t})^T$, and $b_{1i} = b_{2i} = 0$, $i = 1, 2, 3$, $b_{31}(Y_t) = -2\alpha\chi_1 Y_{2,t}$, $b_{32}(Y_t) = -\omega^2\chi_2 Y_{1,t}$, $b_{33}(Y_t) = \chi_3$. The term $2\alpha^2\chi_1^2 Y_{2,t}$ appearing in the expression for $a_2(Y_t)$ is a Wong-Sakai correction term [27].

Example 6 - Dimentberg I

The following set of parameters has been chosen, which comply with the condition of equation (42): $\alpha = 0.1$, $\beta = 0.4$, $\omega = 1.0$, $\gamma_1^2 = 5.0$, $\gamma_2^2 = 0.2$ and $\gamma_3^2 = 0.3$. Figure 15 shows the analytical and numerical PI results in the form of marginal stationary PDFs. The agreement between the two sets of results is seen to be very good.

For concenience, most of the PI calculations have been carried out with equidistant grids. Clearly, this may not be the optimal choice in terms of the accuracy to CPU time ratio. In many cases this can be improved by adopting non-equidistant grids. This effect is illustrated by Figure 16, which corresponds to Figure 15, but the PI results are calculated on the basis of a non-equidistant 15×15-grid. The accuracy is practically the same as in Figure 15, but the reduced grid leads to a reduction of required CPU time by a factor of almost 3.

Example 7 - Dimentberg II

This example is determined by the following set of parameters: $\alpha = -0.1$, $\beta = 0.1$, $\omega = 1.0$, $\gamma_1^2 = 0.1$, $\gamma_2^2 = 0.1$ and $\gamma_3^2 = 0.3$. In Figure 17 are given the results for the stationary PDFs (marginal) from both the PIS and the Monte Carlo simulations. The agreement between the two methods are good where comparison is feasible. Figure 18 shows 3D-plots of the stationary joint PDFs by numerical PI and Monte Carlo simulation.

8 STOCHASTIC DIFFERENTIAL EQUATIONS WITH α-STABLE LÉVY PROCESSES

Due to an increasing interest in exploring the use of α-stable stochastic processes for modeling physical and economic processes, the purpose of this section

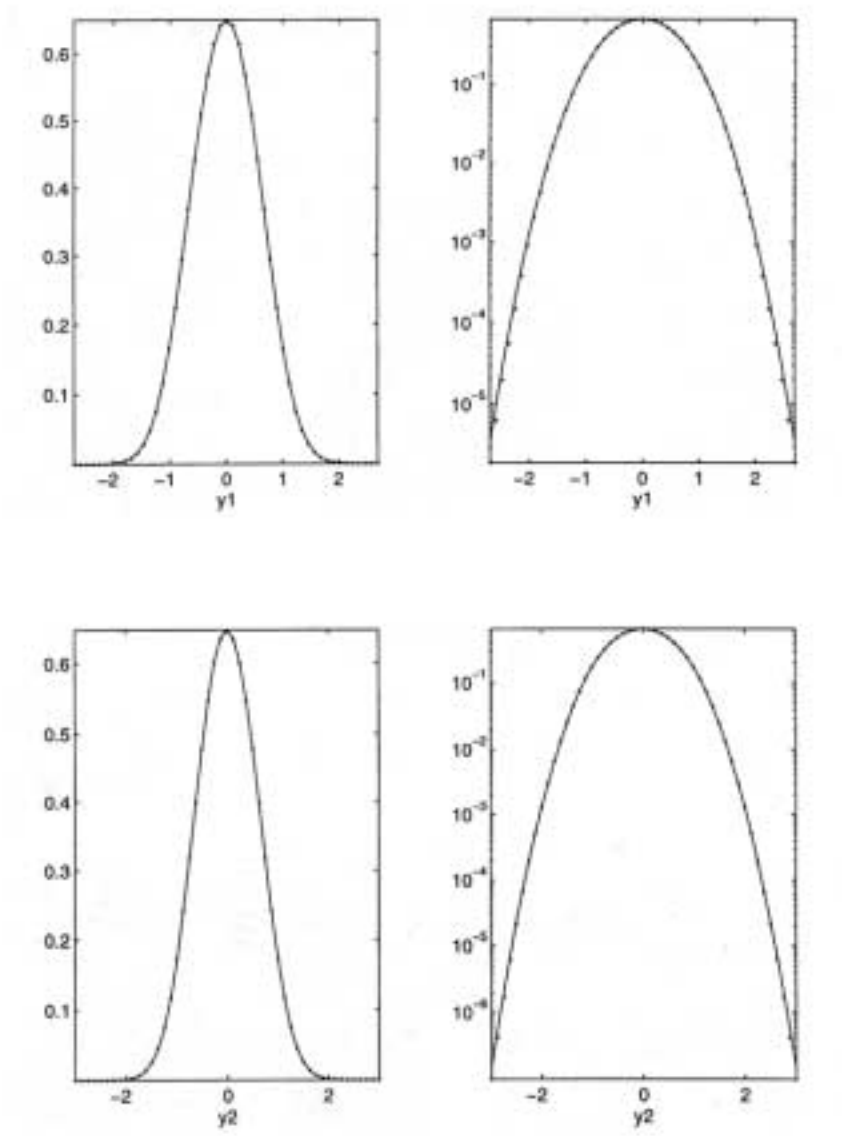

Figure 15: Linear and logarithmic plots of exact (solid line) vs. numerical PI with equidistant 25×25 -grid ($\bullet$ $\bullet$ $\bullet$) results using Splines B for the marginal stationary response PDF of the 2D Dimentberg oscillator (Example 6). Top figures: Displacement. Bottom figures: Velocity

is to describe some initial efforts to explore the potential of the PI technique for calculating the PDF of the state space vector of various SDEs with α-stable Lévy noise [37].

The SDE is still considered as an (extended) Itô SDE, and it is written in the following form

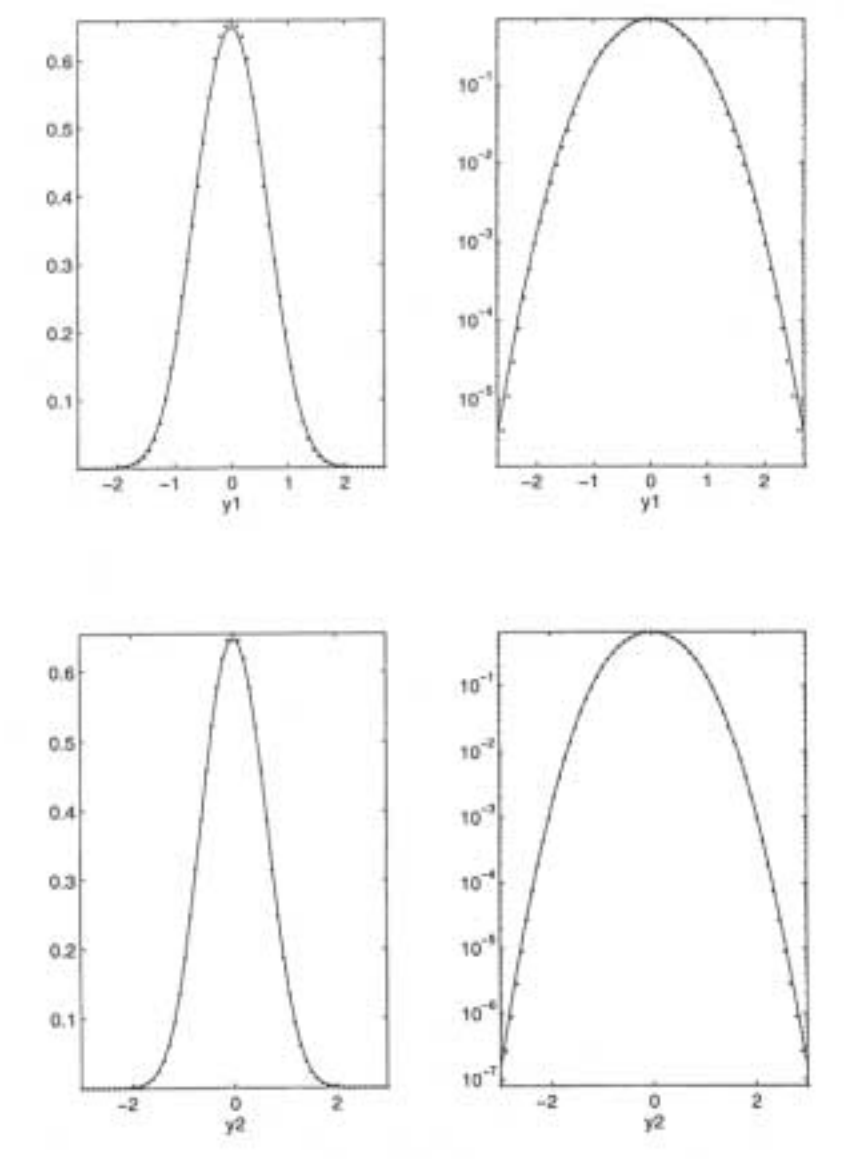

Figure 16: Linear and logarithmic plots of exact (solid line) vs. numerical PI with non-equidistant 15×15 -grid ($\bullet$ $\bullet$ $\bullet$) results using Splines B for the marginal stationary response PDF of the 2D Dimentberg oscillator (Example 6). Top figures: Displacement. Bottom figures: Velocity

$$dY_t = a(Y_t)\,dt + b(Y_t)\,dL_t^{(\alpha)} \tag{45}$$

where $Y_t =$ the (n-dimensional) state space vector process, and $L_t^{(\alpha)}$, $0 < \alpha \leq 2$, is a scalar α-stable Lévy motion process, cf. [38]. When $\alpha = 2.0$, $L_t^{(\alpha)}$ becomes a Brownian motion. $a(Y_t)$ and $b(Y_t)$ are defined as in the standard case.

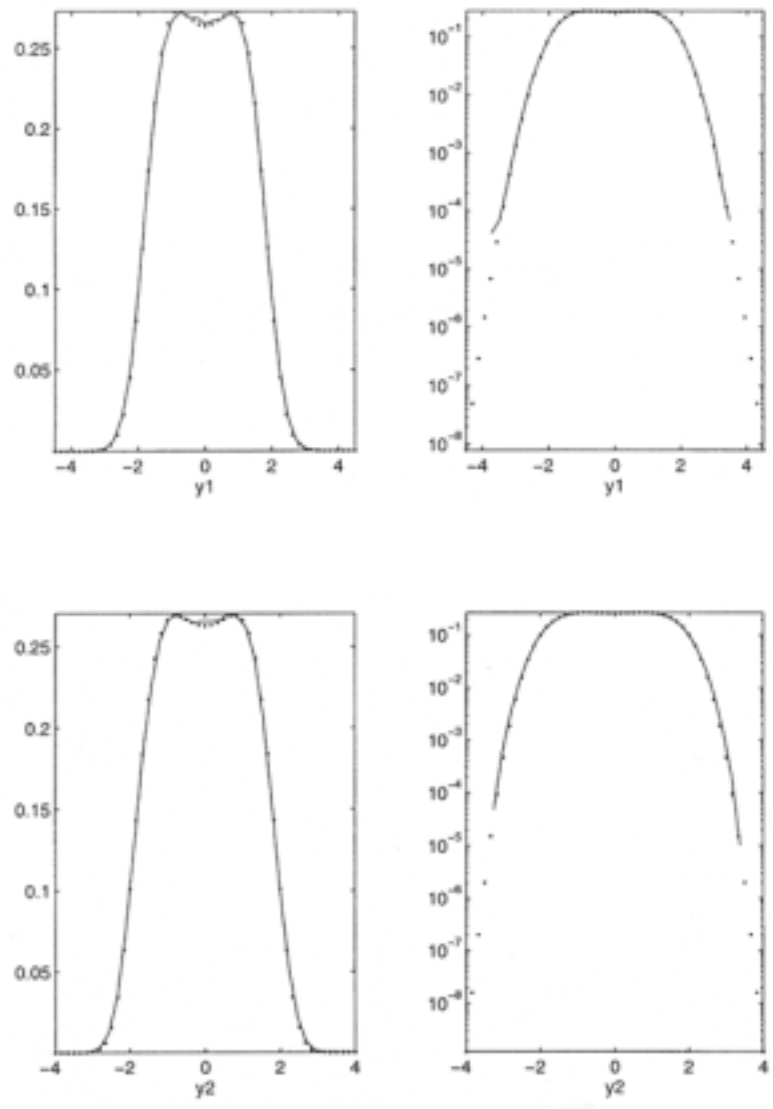

Figure 17: Linear and logarithmic plots of Monte Carlo (solid line) vs. numerical PI with equidistant 25×25 -grid ($\bullet$ $\bullet$ $\bullet$) results using Splines B for the marginal stationary response PDF of the 2D Dimentberg oscillator (Example 7). Top figures: Displacement. Bottom figures: Velocity

For the sake of easy reference, a brief overview over some of the basic features of α-stable Lévy processes that is of relevance here will be given.

A (real) random variable X is said to have a stable distribution if there are parameters $0 < \alpha \leq 2$, $\sigma > 0$, $-1 \leq \beta \leq 1$, and μ real such that its characteristic function $\psi(\theta) = E[\exp i\theta X]$ assumes the following form [38].

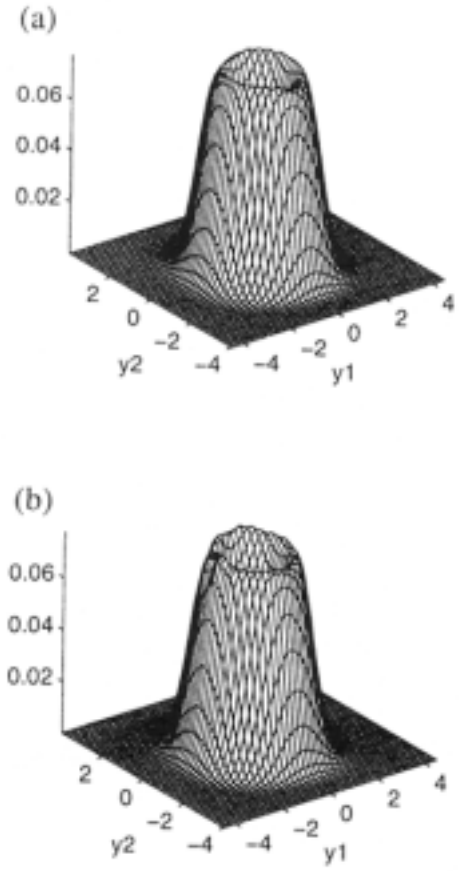

Figure 18: 3D plots of the stationary joint PDF of displacement (y_1) and velocity (y_2) of the 2D Dimentberg oscillator (Example 7). Top figure: Numerical PI with equidistant 25×25 -grid. Bottom figure: Monte Carlo results

If $\alpha \neq 1$:

$$\psi(\theta) = \exp\{-\sigma^\alpha |\theta|^\alpha (1 - i\beta \text{sign}\theta \tan(\pi\alpha/2)) + i\mu\theta\} \tag{46}$$

If $\alpha = 1$:

$$\psi(\theta) = \exp\{-\sigma|\theta|(1 + i\beta(2/\pi)\text{sign}\theta \ln|\theta|) + i\mu\theta\} \tag{47}$$

Here $\text{sign}\theta = 1$ if $\theta > 0$, $= 0$ if $\theta = 0$, $= -1$ if $\theta < 0$. $\alpha =$ the stability parameter, $\sigma =$ the scale parameter, $\beta =$ the skewness parameter, and $\mu =$ the shift parameter. Since the distribution of X is characterized by these four parameters, the notation $X \sim S_\alpha(\sigma, \beta, \mu)$ is often adopted to denote the situation that X is a stable variable with a specified set of parameters. When X is symmetric α-stable, that is $\beta = \mu = 0$, we shall write $X \sim S\alpha S$.

From equation (46) it follows that the stable distribution is Gaussian when $\alpha = 2$ ($\beta = 0$). Then σ is proportional to the standard deviation, and μ equals the mean value. When $\alpha < 2$, the tails of the probability distributions decay like a power function. Specifically, $\lim_{x\to\infty} x^\alpha Prob\{X > x\} = C_\alpha \sigma^\alpha (1+\beta)/2$ and $\lim_{x\to\infty} x^\alpha Prob\{X < -x\} = C_\alpha \sigma^\alpha (1-\beta)/2$, where C_α is a constant [38]. Hence it follows that no finite variance exists when $\alpha < 2$. Such distributions are frequently referred to as having heavy tails. Further, a finite mean value is obtained only if $\alpha > 1$. Such distributions therefore leads to much more variability than a Gaussian distribution. This effect will be demonstrated below.

It may also be noted that the probability density functions (PDF) of α-stable random variables exist and are continuous, but unknown in closed form with few exceptions. When $\alpha < 2$ and $\beta = 0$, only one nontrivial case is known in closed form, viz. the Cauchy distribution $S_1(\sigma, 0, \mu)$. If $X \sim S_1(1, 0, 0)$, then its PDF is given as follows

$$p(x) = \frac{1}{\pi(\, x^2 + 1\,)} \tag{48}$$

For illustration, we shall also investigate the case when $\alpha = 1.5$. A numerical procedure for calculating the PDF is then required. Here we shall use the following result [38]: $X \sim S_\alpha(1, 0, 0)$ if

$$X = \frac{\sin(\alpha\Pi)}{(\cos\Pi)^{1/\alpha}} \left(\frac{\cos((1-\alpha)\Pi)}{W} \right)^{(1-\alpha)/\alpha} \tag{49}$$

where Π is a random variable uniformly distributed on $(-\pi/2, \pi/2)$ and W is an exponential random variable with mean 1. The FORTRAN program *rstable* [38] is used to generate a very large sample of the random variable $X \sim S_{1.5}(1, 0, 0)$ which is then used to determine the PDF with desired accuracy. Figure 19 shows the PDF used for the calculations to be discussed below.

To be able to change the parameters of the PDFs, the following property will be used later. If $X \sim S_\alpha(1, 0, 0)$, and $\sigma > 0$ and μ are real constants, then $\sigma X + \mu \sim S_\alpha(\sigma, 0, \mu)$.

The stochastic process $L_t^{(\alpha)}$ $(t \geq 0)$ is a (symmetric) α-stable Lévy motion process if

1. $L_0^{(\alpha)} = 0$ (a.s.),
2. $L_t^{(\alpha)}$ has independent increments,
3. $L_t^{(\alpha)} - L_s^{(\alpha)} \sim S_\alpha(\,(t-s)^{1/\alpha}, 0, 0)$ for any $0 \leq s < t < \infty$ and $0 < \alpha \leq 2$.

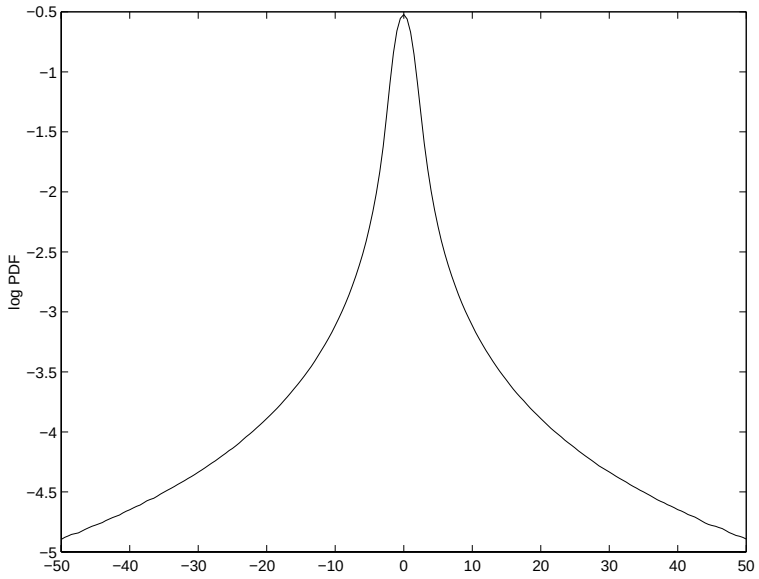

Figure 19: The PDF of $X \sim S_{1.5}(1, 0, 0)$

It follows that such a process has stationary increments, and it becomes a Brownian motion for $\alpha = 2$. Also, for fixed t, $L_t^{(\alpha)} \sim S\alpha S$.

The distinct difference between a Brownian motion $L_t^{(2)}$ on the one hand and the Cauchy motion $L_t^{(1)}$ and $L_t^{(1.5)}$, on the other, is displayed in Figures 20-22, which shows part of a realization of each of these processes. In contrast to the Brownian motion, a typical feature of the two other processes is the sudden large excursions, which tend to become more pronounced with decreasing α-parameter. This reflects the much larger variability inherent in e.g. the Cauchy distribution as opposed to the Gaussian law which determine the variability in the Brownian motion.

It is clear that the PI solution of a standard SDE with Brownian motion detailed in previous sections can be adapted almost word for word to also apply to the extended SDE with α-stable Lévy motion. However, as already seen, for $\alpha < 2.0$, only for the case of Cauchy motion does there exist a closed form expression for the TPD. For the other values of $\alpha < 2$, a normalized, empirical PDF can easily be produced and stored, and only rescaling and shifting is needed to provide the required TPD.

We shall conclude by calculating the stationary PDF of the following dynamic model

$$\ddot{X}_t + 2\xi\dot{X}_t + X_t + \lambda X_t^3 = 2\sqrt{\xi}\, N_t^{(\alpha)} \tag{50}$$

where $\Delta L_t^{(\alpha)} = N_t^{(\alpha)}\, \Delta t$. So this model can be recognized as a Duffing oscillator driven by an α-stable Lévy white noise. For the numerical calculations, which

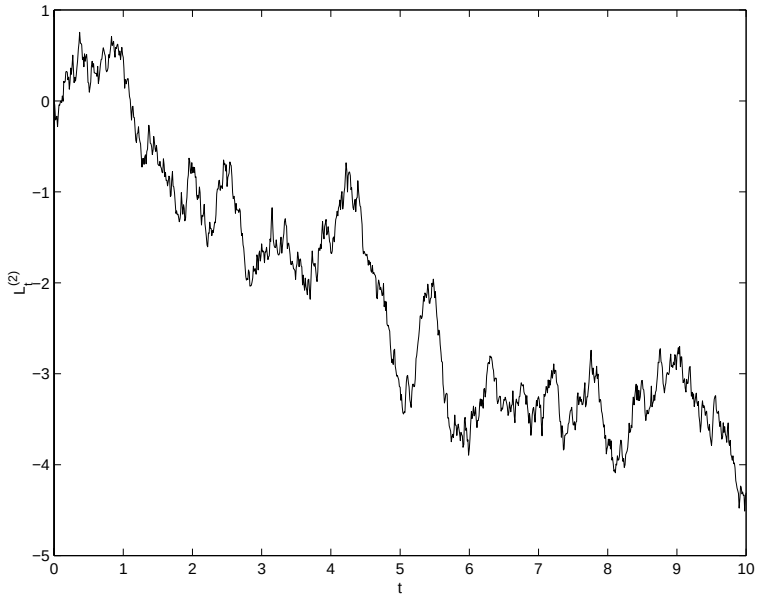

Figure 20: A realization of α-stable Lévy motion $L_t^{(2)}$, i.e. Brownian motion

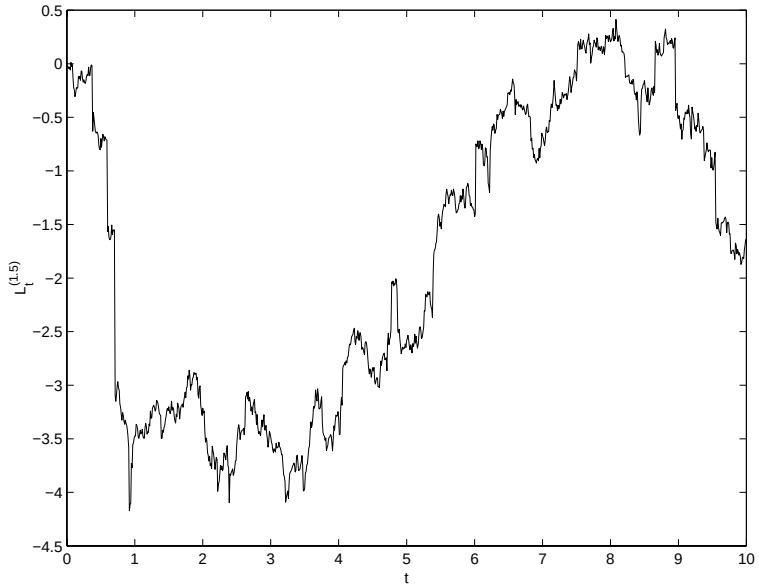

Figure 21: A realization of α-stable Lévy motion $L_t^{(1.5)}$

were based on Splines A 31×31 grid. The parameter values were $\xi = 0.25$ and $\lambda = 0.2$, the same as in previous examples.

One of the specific problems that one has to cope with in a numerical calculation of the joint PDF of the state space vector of dynamic systems

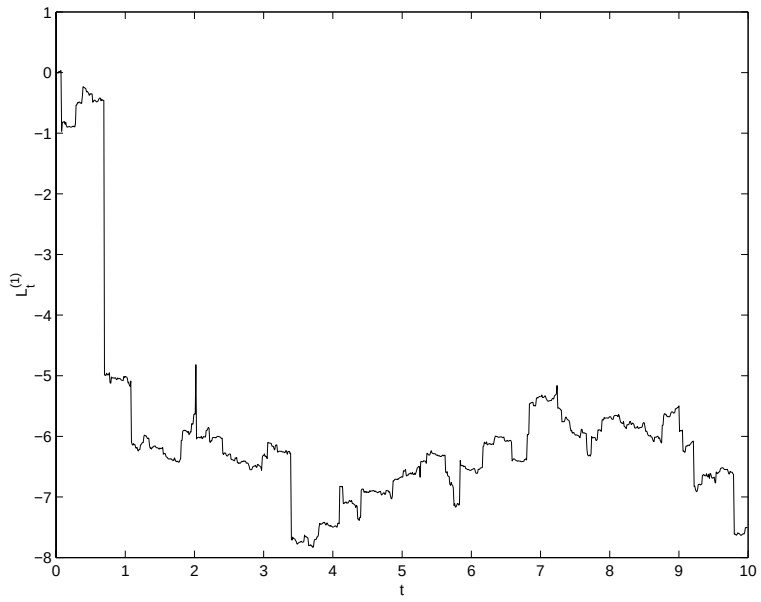

Figure 22: A realization of α-stable Lévy motion $L_t^{(1)}$, i.e. Cauchy motion

driven by an α-stable Lévy white noise with $\alpha < 2$, is the extension of the domain in state space where the PDF needs to be considered to obtain accurate results by PI. The heavy tails of the PDF of the excitation process is of course reflected in the tails of the PDF of the response process. Compared to the case of Gaussian white noise driven oscillators, in general a much larger domain has to be considered. However, this is compensated by the small gradients associated with the PDF of the response process, which allows a discretization of the state space with a comparable number of grid points as in the case of Gaussian white noise excitation.

Example 8 - $\alpha = 1.5$

For this case, the choice of domain was $[-30, 30] \times [-35, 35]$ with 31 grid points on each axis. The number of grid points is very similar to what was required for Gaussian white noise excitations while the domain is much larger. To get a check on the results, extensive Monte Carlo simulations were carried out to obtain accurate estimates of the joint PDF also in the tail region. It is found that reasonable accuracy is obtained over almost the entire domain except at the boundary of the domain. This is illustrated by the plots in Figure 23 where the maginal PDF of displacement and velocity response obtained by PI and Monte Carlo simulations are shown.

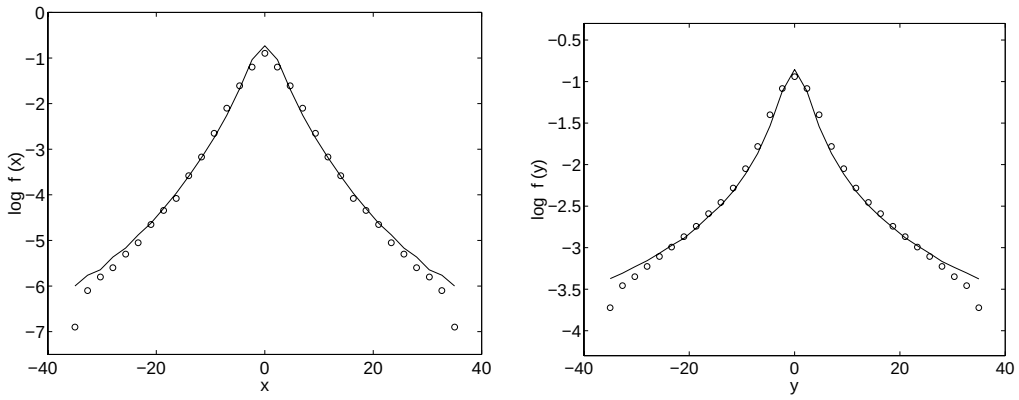

Figure 23: The marginal PDF of stationary response obtained by PI (∘)and Monte Carlo simulations (−−) for $\alpha = 1.5$. Left figure: Displacement. Right figure: Velocity.

Example 9 - $\alpha = 1.0$

For the case $\alpha = 1.0$, that is, Cauchy motion, the chosen domain was $[-35, 35] \times [-35, 35]$ also with 31 grid points on each axis. In this case very good agreement was found over the entire domain between the joint PDF obtained by PI and extensive Monte Carlo simulations. Figure 24 show the maginal PDF of displacement and velocity response obtained by PI and Monte Carlo simulations. Also for this case, good numerical accuracy is obtained.

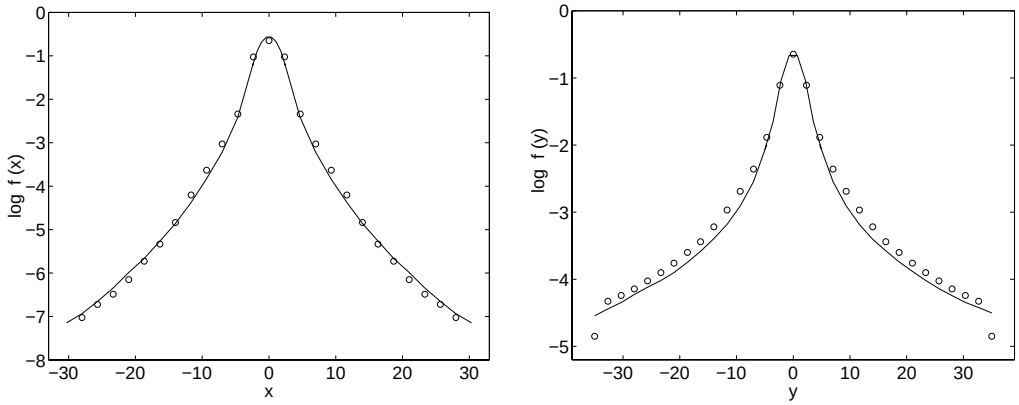

Figure 24: The marginal PDF of stationary response obtained by PI (•)and Monte Carlo simulations (−−) for $\alpha = 1.0$. Left figure: Displacement. Right figure: Velocity.

9 Acknowledgements

These lecture notes are based on work carried out during three doctoral projects at NTNU in Trondheim over a period of roughly ten years. Three main contributors to the development of the methods detailed here are therefore the three doctoral students involved, viz. John Magne Johnsen [39], Vibeke Moe [34] and Christian Skaug [40]. All the numerical results shown are due entirely to their efforts.

References

[1] Risken H. The Fokker-Planck Equation. Second Edition. Berlin: Springer-Verlag, 1989.

[2] Caughey TK, Ma F. The exact steady-state solution of a class of non-linear stochastic systems. International Journal of Nonlinear Mechanics 1982;17(3):137-142.

[3] Yong Y, Lin YK. Exact stationary response solution for second order nonlinear systems under parametric and external excitations. Journal of Applied Mechanics 1987;54:414-418

[4] Soize C. The Fokker-Planck Equation for Stochastic Dynamical Systems and its Explicit Steady State Solutions. London: World Scientific, 1994.

[5] Langley R. A finite element method for the statistics of non-linear random vibration. Journal of Sound and Vibration 1985;101(1):41-54.

[6] Langtangen HP. A general numerical solution method for Fokker-Planck equations with applications to structural reliability. Probabilistic Engineering Mechanics 1991;6(1):33-48.

[7] Spencer BF, Bergman LA. On the numerical solution of the Fokker-Planck equation for nonlinear stochastic systems. Nonlinear Dynamics 1993;4:357-372.

[8] Wojtkiewicz SF, Bergman LA, Spencer BF. High Fidelity Numerical Solutions of the Fokker-Planck Equation. Proceedings 7th Int. Conf. Structural Safety and Reliability, Kyoto, Japan, Nov. 1997.

[9] Sun JQ, Hsu CS. The generalized cell mapping method in nonlinear random vibration based upon short-time Gaussian approximation. Journal of Applied Mechanics 1990;57:1018-1025.

[10] Naess A, Johnsen JM. Response Statistics of Nonlinear Dynamic Systems by Path Integration. In Bellomo N, Casciati F, editors. Proceedings IUTAM Symposium on Nonlinear Stochastic Mechanics, Turin, July 1991. Berlin: Springer-Verlag, 1992: 401-414.

[11] Naess A, Johnsen JM. Response statistics of nonlinear, compliant offshore structures by the path integral solution method. Probabilistic Engineering Mechanics 1993;8(2):91-106.

[12] Yu JS, Cai GQ, Lin YK. A New Numerical Scheme for Path Integration Method. Proceedings 3rd Int. Conference on Stochastic Structural Dynamics. San Juan, Puerto Rico.

[13] Naess A, Moe V. New Techniques for Path Integral Solution of the Random Vibration of Nonlinear Oscillators. In Shiraishi , Shinozuka M, Wen YK, editors. Proceedings 7th Int. Conference on Structural Safety and Reliability, Kyoto, 1997. Rotterdam: Balkema 1998.

[14] Bhandari RG, Sherrer RE. Random vibrations in discrete nonlinear dynamic systems. Journal of Mechanical Engineering Science 1968;10:168-174.

[15] Atkinson JD. Eigenfunction expansion for randomly excited non-linear systems. Journal of Sound and Vibration 1973;30(2):153-172.

[16] Wen YK. Approximate method for nonlinear random vibration. Journal of the Engineering Mechanics Division, ASCE 1975;101(EM4):389-401.

[17] Dunne JF, Ghanbari M. Extreme-value prediction for non-linear stochastic oscillators via numerical solutions of the stationary FPK equation. Journal of Sound and Vibration 1997; 206(5): 697-724.

[18] Wedig WV, von Wagner U. Extended Laguerre polynomials for nonlinear stochastic systems. In Spanos PD, editor. Proceedings 3rd Int. Conference on Computational Stochastic Mechanics, Santorini, June 1998. Rotterdam: Balkema 1999.

[19] Wehner MF, Wolfer WG. Numerical evaluation of path-integral solutions to Fokker-Planck equations. Physical Review A 1983;27(5):2663-2670.

[20] Wehner MF, Wolfer WG. Numerical evaluation of path-integral solutions to Fokker-Planck equations. II. Restricted stochastic processes. Physical Review A 1983;28(5):3003-3011.

[21] Wehner MF, Wolfer WG. Numerical evaluation of path-integral solutions to Fokker-Planck equations. III. Time and functionally dependent coefficients. Physical Review A 1987;35(4):1795-1801

[22] Guckenheimer J, Holmes P. Nonlinear Oscillations, Dynamical Systems, and Bifurcations of Vector Fields. New York: Springer-Verlag, 1983.

[23] Wiggins, S. Introduction to Applied Nonlinear Dynamical Systems and Chaos. New York: Springer-Verlag 1990.

[24] Lasota A, Mackey MC. Chaos, Fractals and Noise, Second Edition. New York: Springer-Verlag 1994.

[25] Rudin, W. Real and Complex Analysis, 3rd Edition. New York: McGraw-Hill Book Comp., 1987.

[26] Ulam SM, von Neuman J. On combination of stochastic and deterministic processes. Bull. Am. Math. Soc., 1947;53:723-738.

[27] Wong E, Hajek B. Stochastic Processes in Engineering Systems. New York: Springer-Verlag, 1985.

[28] Øksendal B. Stochastic Differential Equations. Fifth Edition. Berlin: Springer-Verlag, 1998.

[29] Naess A, Moe V. Efficient path integration methods for nonlinear dynamic systems. Probabilistic Engineering Mechanics, 2000;15:221-231.

[30] Kloeden PE, Platen E. Numerical Solution of Stochastic Differential Equations. Berlin: Springer-Verlag, 1992.

[31] Hsu CS. A Generalized Theory of Cell-to-Cell Mapping for Nonlinear Dynamical Systems. Journal of Applied Mechanics, ASME, 1981;48:634-642.

[32] Crandall SH, Chandiramani KL, Cook RG. Some First-Passage Problems in Random Vibrations. Journal of Applied Mechanics, 1966;33:532-538.

[33] de Boor C. A Practical Guide to Splines. New York: Springer-Verlag, 1978.

[34] Moe V. Nonlinear random vibrations - numerical analysis by path integration methods. PhD dissertation, Norwegian University of Science and Technology, Trondheim, 1997.

[35] Caughey TK. Nonlinear Theory of Random Vibrations. Advances in Applied Mechanics 1971:209-253.

[36] Dimentberg MF. An exact solution to a certain non-linear random vibration problem. International Journal of Non-Linear Mechanics 1982;17(4):231-236.

[37] Naess A, Skaug C. Extension of the Numerical Path Integration Method to Filtered α-stable Lévy Noise. Proceedings 3rd International Conference on Computational Stochastic Mechanics. Rotterdam: Balkema, 1999.

[38] Samorodnitsky G, Taqqu MS. Stable Non-Gausian Random Processes, New York: Chapman and Hall, 1994.

[39] Johnsen JM. Response Statistics of Nonlinear Dynamic Systems. PhD dissertation, Norwegian University of Science and Technology, Trondheim, 1992.

[40] Skaug C. Random Vibration and the Path Integral Method. PhD dissertation, Norwegian University of Science and Technology, Trondheim, 2000.